Materials Today Nano 22 (2023) 100329

Contents lists available at ScienceDirect

Materials Today Nano

journal homepage: https://www.evise.com/profile/#/MTNANO/login

Status and perspectives of transparent conductive oxide films for silicon heterojunction solar cells

Wei Cui [a, b, c], Fengjiao Chen [a], Yawen Li [a, d], Xiaodong Su [b, **], Baoquan Sun [a, d, e, *]

[a] Institute of Functional Nano & Soft Materials (FUNSOM), Soochow University, Suzhou, Jiangsu 215123, PR China
[b] School of Physical Science and Technology, Soochow University, Suzhou, Jiangsu 215123, PR China
[c] Research & Development Department, Canadian Solar Inc, 199 Lushan Road, SND, Suzhou 215129, PR China
[d] Jiangsu Key Laboratory of Advanced Negative Carbon Technologies, Soochow University, Suzhou, Jiangsu 215123, PR China
[e] Macau Institute of Materials Science and Engineering, MUST-SUDA Joint Research Center for Advanced Functional Materials, Macau University of Science and Technology, Macau 999078, PR China

ARTICLE INFO

Article history:
Received 28 December 2022
Received in revised form
8 March 2023
Accepted 20 March 2023
Available online 25 March 2023

ABSTRACT

Efficiently harvesting solar energy into electricity *via* photovoltaic devices (also called solar cells) exhibits a feasible way to tackle challenging energy supply. Over the past decades, crystal silicon (c-Si) is still the dominant material for photovoltaic manufacture, benefiting from its nearly ideal optical bandgap, abundant, and mature semiconductor technology. Up to now, the power conversion efficiency of single-junction c-Si solar cells with heterojunction structures has been boosted to over 26%, approaching its theoretical maximum efficiency. On the other hand, a trade-off of the cost/output power of heterojunction cells is still an obstacle to its expanding market share. Being different from any previous scalable c-Si photovoltaic generations, the heterojunction cell features uniquely indispensable transparent conducting oxide (TCO) layers integrating a low-temperature annealing metal paste. Its unique electrode requirement is still the dominant factor to determine its rate of exposure mass manufacture. In this review, the field of TCO development of silicon heterojunction (SHJ) solar cells is overviewed firstly. Furthermore, different TCO choices for SHJ solar cells are discussed. Finally, future research directions, challenges, and potential solutions are summarized and looked forward. To conclude, we discuss what has been taken for the TCO application for SHJ solar cells in the mass market.

1. Introduction

The world market of photovoltaics (PV) is currently dominated by crystal silicon (c-Si)-based solar cells, which occupy a market share of approximately 95% in 2019 [1,2]. Amongst c-Si solar cells, aluminum back surface field (Al-BSF) cells and passivated emitter and rear contact (PERC) cells (Fig. 1a), which are also named by homojunction c-Si solar cells, are predominating in large-scale industrial solar cell products (Fig. 1b). However, due to the high carrier recombination at the silicon surface, the values of the power conversion efficiency (PCE) of Al-BSF cells and PERC cells are reaching their limitation, which are around 20% and 24% [3], respectively, as shown in Fig. 1c. Besides, the polysilicon-passivated junction technique, built by embedding a thin silicon oxide layer atop a c-Si substrate, also named tunneling oxide passivated contact (TOPCon), is emerging as a promising alternative. And a record PCE of 26.4% [4] has been achieved in TOPCon cells.

As an alternative, silicon heterojunction (SHJ) solar cell technique is an important approach for the next generation of high-efficiency PV productions [1,6,7], as predicted in Fig. 1d. In the 1990s, Sanyo Co. invented the first SHJ solar cell, which integrated a boron-doped hydrogenated amorphous silicon (a-Si:H) emitter with an n-type c-Si wafer and achieved a PCE close to 12% [8]. And then Sanyo Co. improved the PCE to 22.8% [9] and 23.7% [10] in 2009 and 2011, respectively, in which the carrier concentration of the transparent conducting oxide (TCO) films was reduced to mitigate free carrier absorption (FCA), while the Hall mobility was improved to optimize the lateral conductivity. In 2013, they further enhanced the PCE to 24.7% [11]. And then, the PCE of double-side SHJ solar cells reached 25.1% [12] on a large area device of 151.9 cm^2 by Kaneka Co. in 2015 due to high fill factor (FF) of 83%. An interdigital back-contact (IBC) structure was combined with the

* Corresponding author.
** Corresponding author.
E-mail addresses: xdsu@suda.edu.cn (X. Su), bqsun@suda.edu.cn (B. Sun).

https://doi.org/10.1016/j.mtnano.2023.100329
2588-8420/

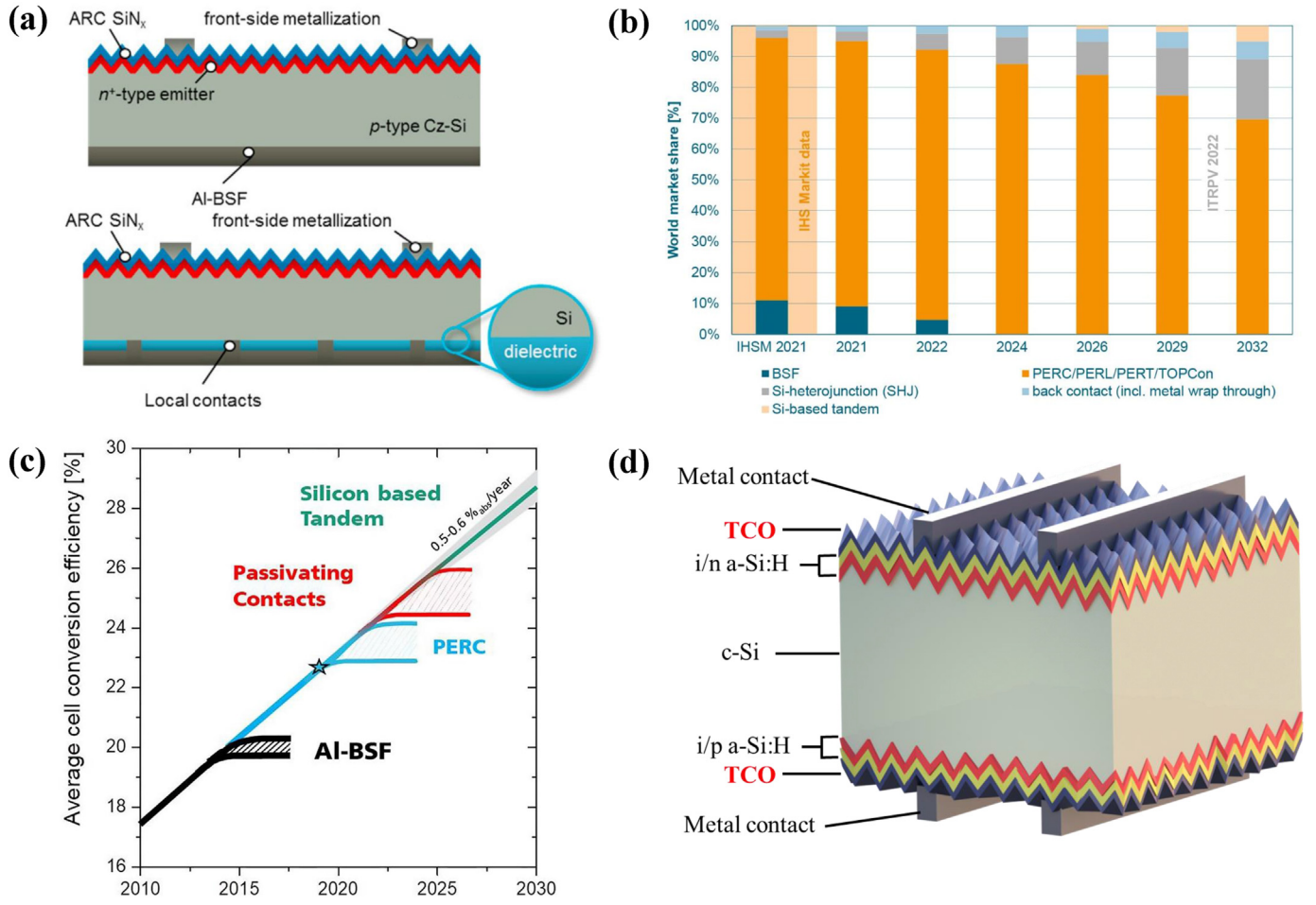

Fig. 1. (a) The schematic of the aluminum back surface field (up) and the passivated emitter and rear contact cells (down) [5]. Copyright 2017, Elsevier. (b) The market share trend of the Si-based solar cells predicted by the International Technology Roadmap for Photovoltaic [2]. (c) The research and development roadmap of c-Si PV productions [3]. Here, a passivating contact mainly consists of a tunneling oxide passivated contact and silicon heterojunction structure c-Si PV. Copyright 2020, The American Institute of Physics. (d) The schematic of silicon heterojunction solar cells.

SHJ solar cells to reduce the parasitic absorption from the a-Si:H and TCO layers, resulting in a record PCE of 26.7% [13] in 2017. In 2022, SHJ solar cells based on transition metal doped indium oxide (IMO) and hydrogenated microcrystalline silicon (μ-Si:H) achieved a PCE of 25.26% [14]. And in the same year, Longi Co. raised the world-record PCE to 26.81% [15] for SHJ solar cells, approaching the fundamental limit of single junction Si solar cells (29.4%) [16]. In recent years, several industry players joined the SHJ solar cell market. As predicted by the International Technology Roadmap for Photovoltaic [2], SHJ cells are expected to gain a market share of about 10% in 2025, corresponding to a shipment of over 100 GW per year. In future mass manufacture, due to the relatively low temperatures in fabrication processes, SHJ solar cells can tolerate continually thinner c-Si thickness (up to 80 μm), which would exactly cater to the cost reduction for the PV industry.

Due to the poor lateral conductivity of the doped a-Si:H layers in SHJ solar cells, the front and rear sides of the devices must be combined with transparent electrode layers to deliver the photogenerated charges to the terminals. Amongst all the materials for the transparent electrodes, TCOs are ideal candidates to meet the requirement. TCOs are intrinsically wide band-gap materials, typically metal oxides, that can be heavily doped and serve as transparent conductors for charge carrier extraction at the device terminals [17–22]. Since the 1960s and 1970s, TCOs have witnessed the revolutionary development of SHJ solar cells due to their outstanding electronic and optical properties [23–26]. Existing reviews on this topic either emphasize all aspects of SHJ solar cells or are out of date [1,7,27–29]. In other works, researchers reviewed the achievements and the challenges of TCO films [30–32]. As TCOs are fundamental materials for SHJ solar cells, a systematic review of material selection, characterization, and gigawatt-scale production is essential but still lacking. This article reviews the general requirements and the status of the development of TCO films targeting high-performance SHJ solar cells. In the first section, we listed and discussed the relevant properties of TCO films for the application in SHJ solar cells, including conductivity, transparency as well as contact resistance at the interfaces. Additionally, we also elucidated the influence factors and the control strategies for the passivation detrimental effect during the deposition of TCO films. In the second section, we summarized the application of various TCOs in the field of SHJ solar cells, focusing on their influence on work function (WF), resistivity, and transmittance on the performance of SHJ solar cells. In the third section, we presented the current state and developing trend of TCO films in the industrialization of SHJ solar cells.

2. Application requirements of TCO films in SHJ solar cells

2.1. Transparency, reflectance, and conductivity of TCO films

In SHJ solar cells, both optical and electrical properties are significant for TCO films. However, there is always a trade-off between these two properties. The improvement of the transparency of the

TCO films always leads to the reduction of the conductivity, and *vice versa*. Therefore, it is important to make a balance between the optical and electrical properties of TCO films to achieve desirable performance in SHJ solar cells.

As bifacial devices, the performance of SHJ solar cells is primarily influenced by the optical properties of the TCO films, including transparency and antireflection (AR) properties, at both the front and rear sides. The transparency of the TCO films is mainly determined by the band structure and the deposition condition [33]. For application in SHJ solar cells, the material should possess decent transmittance in the visible and near-infrared spectral range. For this reason, typical metal oxides with a fundamental bandgap larger than 3 eV [33,34], including indium oxide (In_2O_3) [35], tin oxide (SnO_2) [36,37], and zinc oxide (ZnO) [35,38], are widely applied in TCO films. To improve their conductivity, the metal oxides are doped by other elements to shift the Fermi level into the conduction band, during which the free carrier concentration (N_e) in the oxides is improved. The transmittance toward the long wavelength region is tremendously affected by N_e. According to Drude theory, the plasma frequency ω could be written as Equation (1) [39,40]:

$$\omega^2 = \frac{e^2 \cdot N_e}{\varepsilon_0 \cdot \varepsilon_r \cdot m^*} \tag{1}$$

where, e is the electric charge carried by a single electron, and ε_0 and ε_r are the vacuum and relative permittivity, respectively. The plasma frequency defined the onset of the FCA, thus the increase of N_e would reduce the transmittance of the TCO films at a long wavelength range.

Generally, TCO films also act the role of AR coatings, which determines the thickness of the films. The reflectance on the Si surface is minimized for one wavelength, which is given by Ref. [33]:

$$d_{TCO} = \frac{\lambda}{4n} \tag{2}$$

where, λ is the wavelength at which the reflectance is minimized, n is the refractive index of the TCO films at the wavelength, and d_{TCO} is the thickness of the TCO films. Generally, to achieve the best PCE performance, the solar cell should present the lowest reflectance at the visible light range (400–760 nm), which determines the thickness of the TCO films. For example, for indium tin oxide (ITO) films on the front side of the SHJ solar cells, the thickness is generally set at 70–80 nm since ITO exhibits an n of approximately 1.9 at the wavelength of 580 nm [41]. For the TCO films on the rear sides, the thickness could be a bit larger to mitigate the sheet resistance (R_{sheet}) at the cost of reducing the PCE measured at the rear side (for bifacial cells).

In SHJ solar cells, the R_{sheet} of the TCO films determines the pitch of the metal grids. A decrease of R_{sheet} allows a larger pitch of the metal grid, which then benefits the cell performance by reducing themetal shading area as well as improving lateral transportation. Since R_{sheet} is defined as $R_{sheet} = \rho/d_{TCO}$, either reducing electrical resistivity (ρ) or accumulating d_{TCO} enables R_{sheet} smaller. However, as discussed above, d_{TCO} is determined mainly by the anti-reflectance performance. In the TCO films, the relationships among resistivity ρ, N_e, and the carrier mobility (μ) could be described as Equation (3) [42],

$$\rho = \frac{1}{eN_e\mu} \tag{3}$$

Either the improvement of N_e or μ leads to a decrease in ρ, which further reduces R_{sheet} and improves *FF* in solar cells. Most TCO materials are n-type semiconductors, and N_e of their films is primarily determined by the dopant concentration in the host materials. Besides, N_e could also be tuned by deposition conditions, such as deposition power [43], the pressure of the chamber [44], partial pressure of oxygen [45–47] and water [48,49] etc, which results in a value of N_e in the range from 10^{19} to 10^{21} cm^{-3} [50]. Since the increase of N_e degrades the transparency of the TCO films in the visible and near-infrared region, the best strategy to reduce R_{sheet} is to increase μ while limiting N_e. The μ in n-type materials could be written as Equation (4) [33,51],

$$\mu = \frac{e\tau}{m^*} \tag{4}$$

where, τ is the relaxation time and m^* is the effective mass of an electron in the conduction band, respectively. Different scattering mechanisms caused by ionized impurities, neutral impurities, or gain boundaries have an impact on the relaxation time of the carriers in the TCO films and decrease μ [33,51]. For the ITO films applied in SHJ solar cells, typical motilities are 20–40 $cm^2/(V \cdot s)$ [35,52].

Therefore, as the aspect of the solar cell performance, it is a trade-off between the transparency and the conductivity of the TCO films. The increase of N_e leads to an improvement in conductivity but a reduction in transparency, while the decrease results in a contrary result. To balance the optical and the electrical properties of the TCO films, the figure of merit (Φ_{TC}) is intruded to evaluate the influence of the films on solar cell performance, which is defined as Equation (5) [53]:

$$\Phi_{TC} = \frac{T_{avg}^{10}}{R_{sheet}} \tag{5}$$

With the T_{avg} the average of the transmittance of the films. The larger Φ_{TC} means a better compromise between the transparency and the conductivity of the TCO films, which leads to better performance of the solar cells.

2.2. Carrier transportation at TCO interfaces

In the structure of SHJ solar cells, TCO films connect the carrier selective layers and the metal electrodes, enabling the TCO films important roles in carrier transportation at the interfaces. Amongst all the interfaces in SHJ solar cells, the carrier transportation at the TCO/doped a-Si:H interfaces has a critical contribution to the series resistivity losses [54,55]. To study the contact resistivity (ρ_c) at the interfaces, the TCO/doped a-Si:H contacts are generally considered as Schottky contacts, in which the carrier transportation is typically governed by the energy band alignment [56,57]. According to simulation results, the WF difference between the TCO film and the a-Si:H layer has a strong influence on the contact resistance [58,59]. That means the WF requirements for the TCO films of the electron contact (TCO/a-Si(n)) and the hole contact (TCO/a-Si(p)) are different. As reported by Ritzau et al. [56], as shown in Fig. 2a, for the ideal electron contacts, the WF of the TCO films should be lower than 4.2 eV, which is close to the Fermi level of the a-Si:H(n) layers. While for the hole contacts at the TCO/a-Si:H(p) interfaces, the WF of the TCO films should be higher than that of the a-Si:H(p) layers (~5.3 eV) [60].

However, the TCO materials applied in SHJ solar cells are typically n-type semiconductors with relatively low WFs, such as ITO (4.2–4.5eV) [36,37], aluminum-doped zinc oxide (AZO) (3.4–4.5eV) [61], etc, which do not meet the requirements for the hole contacts. As illustrated in Fig. 2b, the patterns with the a-Si:H(p)/ITO or a-Si:H(p)/AZO contact exhibit lower open circuit voltages (V_{OC}s) at high illumination intensity than the ones with a

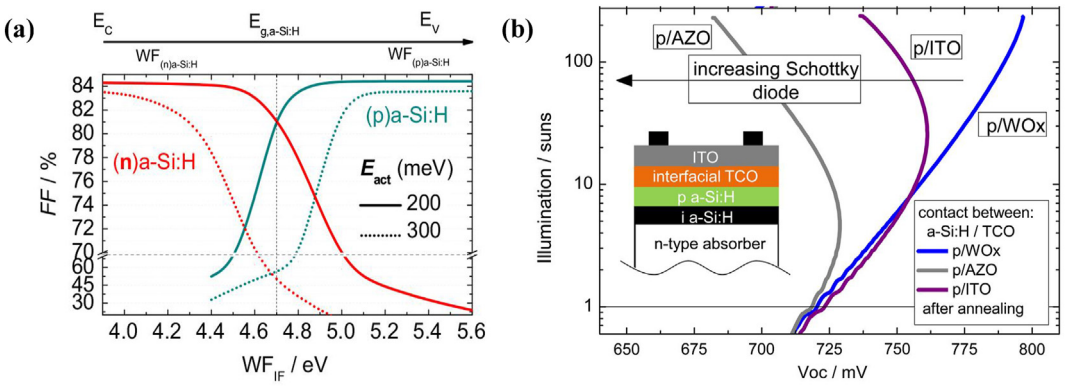

Fig. 2. (a) The simulated fill factor as a function of the work function and a-Si:H doping (n/p type) [56]. (b) Patterns of *Suns-V_{OC}* measurements (open circuit voltages measured with different illumination) of the p-contact at high illumination intensity (the inset is the respective structure in the measurements) [56]. Copyright 2014, Elsevier.

high WF WO_x layer, confirming that large Schottky barriers are formed in the former contacts and hinder carrier transportation at the interfaces. To suppress ρ_c of the hole contacts, high WF transition metal oxides, such as molybdenum oxides (MoO_x) [61–63], tungsten oxides (WO_x) [61,64,65], and vanadium oxides (VO_x) [66], are integrated into SHJ solar cells as contact modification layers. Regarding the a-Si:H(p) layers, a sufficiently high net doping concentration is necessary to optimize ρ_c by avoiding the hole-selective layer from being depleted [55,67,68]. But the rising of the doping concentration burdens the defect densities in the a-Si:H layers [69,70], fixing the effective net doping at a level below 10^{17} cm^{-3}. To realize this strategy, doped hydrogenated nano- or microcrystal-Si (nc-Si:H [68,71] or μc-Si:H [14]) layers, in which the effective net doping level could be higher than 10^{19} cm^{-3}, are integrated into SHJ solar cells, alternating the doped a-Si:H layers. Zhao et al. reported SHJ solar cells with the nc-Si:H(p)/ITO contact and achieved low contact resistance (ρ_c of 0.144 Ω•cm^2) successfully [72].

As discussed above, the traditional transportation exploration at the TCO/doped a-Si:H contacts is mainly based on direct tunneling (DT), which is highly dependent on energy alignment. While in recent works, besides the DT mode, indirect tunneling (IDT) modes, such as trap-assisted tunneling (TAT) and band-to-band tunneling (B2BT), are taken into consideration as well in the simulation of charge carrier transportation at the hole and the electron contacts in SHJ solar cell. Fig. 3a and b show typical carrier transport processes based on the DT and IDT modes at the n- and the p-contact. At the n-contact, the carrier transportation is primarily dominated by the DT mode and supported by TAT mode partially. While at the p-contact, the IDT mode is the dominant one instead of the DT mode. Regarding carrier transportation by either DT or IDT, the charge N_e of TCO films plays an important role. On the one hand, the increase of N_e leads to the decrease of the WFs of TCO films [73], which benefits DT at the electron contact but deteriorates the WF mismatch at the hole contact. On the other hand, larger N_e is beneficial for IDT on both sides of the solar cells [70,73,74]. Therefore, large N_e in TCO films is helpful to maintain low ρ_c at the electron contact areas. While for the hole contacts, due to the WF mismatch, the carrier transportation at the interfaces is primarily determined by IDT but is also impacted by the energy alignment. So, appropriate N_e of the ITO films is required for the hole contacts with small ρ_c. In Fig. 3c, ρ_c for the hole contacts is plotted against N_e of the TCO films [70]. At the active energy (E_a) of the a-Si:H(p) layer at 275 meV, the lowest ρ_c is located at N_e value of approximately 2×10^{20} cm^{-3}. When the N_e rises above this value, the ρ_c slightly increases due to the WF mismatch, while the ρ_c rises monotonically with the reducing N_e below 2×10^{20} cm^{-3}.

The TCO/metal contacts on both sides of the SHJ solar cells are another important factor that should be taken into consideration. In the manufacture of SHJ solar cells, screen printing with low-temperature sintering metal pastes is the most widely applied technique for metallization. During this process, silver (Ag) or silver-coated copper (Ag@Cu) pastes are printed on the TCO surfaces, and metal grid electrodes are formed after drying and sintering processes with temperatures less than 200 °C. Generally, the ρ_c of the TCO/silver grid contacts ($\rho_{c,\ TCO/Ag}$) is primarily dominated by the N_e in TCO films [75]. In SHJ solar cells, the TCO/metal contacts are always treated as Schottky contacts [75]. As a highly doped semiconductor ($N_e > 10^{19}$ cm^{-3}), field emission (FE) or thermionic field emission (TFE) is the dominant transportation mode at the contact [75,76]. According to the Schottky metal/semiconductor junction theory, an increase in N_e in TCO films leads to a thinner potential barrier at the TCO/metal interfaces. Hence, the chance of charge carrier tunneling through the barriers should be enhanced, and $\rho_{c,TCO/Ag}$ is reduced accordingly. As shown in Fig. 3d, Schube et al. proved that $\rho_{c,ITO/Ag}$ decreases with the increase of N_e in the ITO layers under similar printing and sintering conditions [77].

2.3. Degradation of passivation during deposition of TCO films

In recent years, deposition techniques with less damage impact on the a-Si:H layers, such as reactive plasma deposition (RPD) [78], atom layer deposition (ALD) [79–81], and sputtering with mirror shape target configuration [82,83], have been investigated to fabricate TCO films in SHJ solar cells. However, conventional pulsed or direct current magnetron sputtering is still the most widely used deposition technique in the mass production of SHJ solar cells, owing to their high deposition rates and scalability. During the sputtering of TCO films, the a-Si:H passivated silicon substrate interacts withthe plasma intensively, and a significant degradation occurs in the passivation interfaces, leading to a reduction of V_{OC} and pseudo-*FF* in the solar cell performance [84]. The detrimental effect during sputtering primarily arises from ultraviolet (UV) light luminescence [85,86] in plasma and ion bombardment [87,88], including ion and neutral particles from plasma gas, sputtering targets, and their compounds [89]. And the passivation quality could be partially recovered after a high-temperature treatment during or after the TCO deposition process [84,86].

UV radiation is believed as a damage source for the a-Si: H passivation in SHJ solar cells for a long time [85,90,91]. During the deposition processes of TCO films, the a-Si:H passivated Si substrates are under the illumination of plasma and damage occurs in the a-Si:H films or at the a-Si:H/c-Si interfaces. In a-Si:H films, the

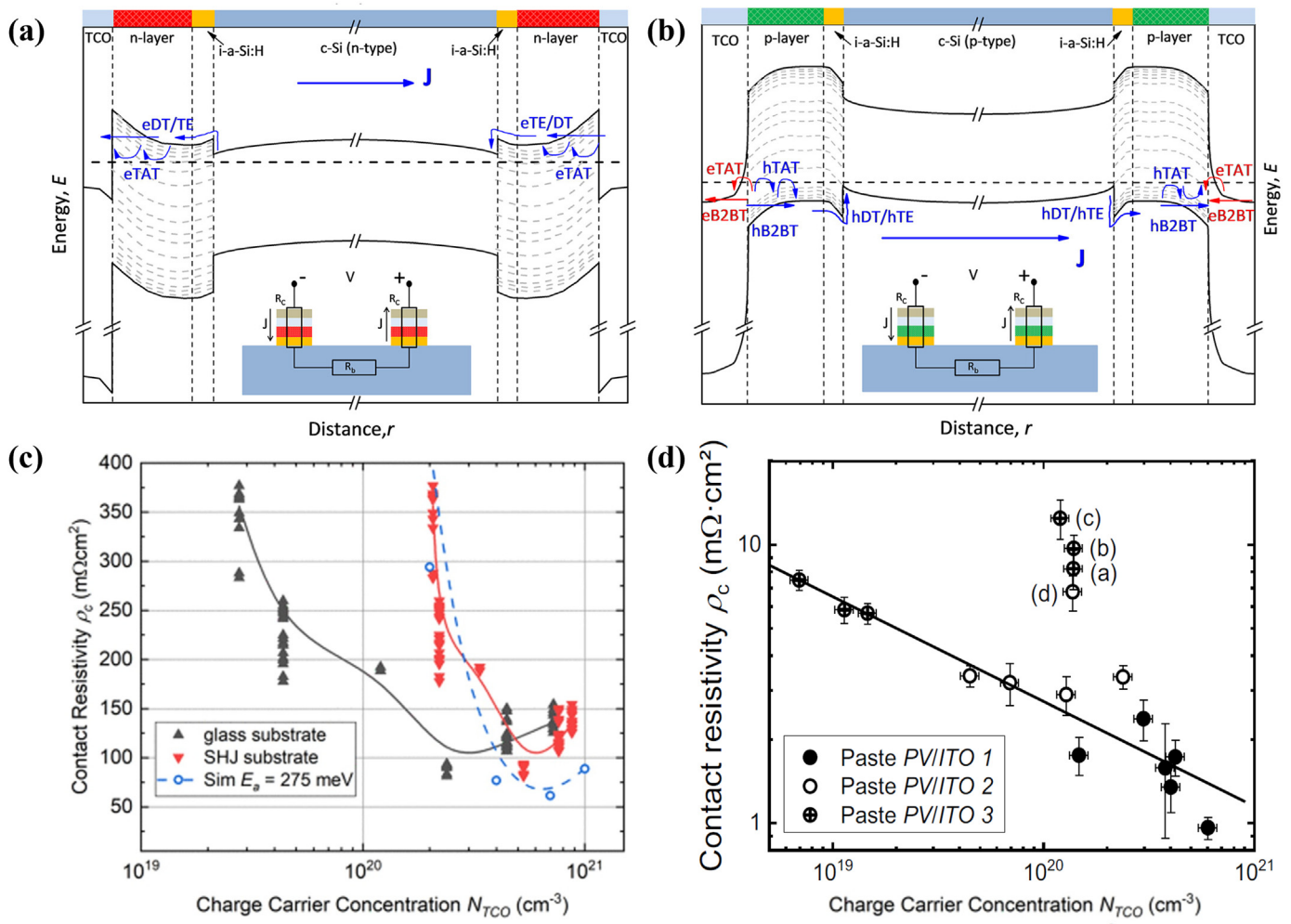

Fig. 3. The schematic band diagrams and carrier transport mechanisms for (a) the n-contact and (b) the p-contact [73]. These mechanisms include the direct tunneling/thermionic emission mode and indirect tunneling modes like trap-assisted tunneling and band-to-band tunneling . Copyright 2020, Wiley-VCH. (c) ρ_c of the hole contact plotted against the carrier concentration of the indium tin oxide (ITO) films (N_{ITO}) measured on glasses or silicon heterojunction substrates after annealing at 200 °C [70]. Copyright 2021, IEEE. (d) Contact resistivity of the ITO/Ag grid contacts as a function of the charge carrier concentration in ITO films (N_{ITO}) [75].

binding energy of Si—H and Si—Si is approximately 3.6 eV [92] and 2.5 eV [93], respectively, which is in the UV—visible spectral range. After the illumination of UV light in plasma, the Si—Si and the Si—H bonds in a-Si:H(i) or a-Si:H/c-Si interfaces are partially broken and then the passivation effect of the Si substrates is degraded [86]. B. Demaurex et al. show that the minority carrier lifetime (MCLT) of the a-Si:H passivated Si samples shielded with normal glasses (10% transparency at 4.7 eV) and quartz glasses (10% transparency at 7.8 eV) dropped 14% and 27% after sputtering, respectively, comparing with a value of 96% on bare samples without shielding [86]. It has been proven that the damage should be ascribed to plasma luminescence. During the plasma illuminating process, the surface recombination velocity of the samples would be degraded after a short exposure of 10 s and reach a saturation value after ~60 s [87]. It was interpreted that the UV light triggers the generation of fast metastable defects at the a-Si: H/c-Si interface in several seconds, and the reversible defects become saturated in a minute.

Ion bombardment is the most critical part of the detrimental effects. During deposition, the MCLT losses of the passivated Si wafer could be more than 90%, as compared with that before deposition [43,84,86,94]. And merely part of the losses could be recovered after annealing. Generally, the detrimental effects of the particle bombardment are correlated with the thickness of the a-Si: H layer [95], the deposition conditions [89,96] as well as the deposition modes [84,97,98]. The a-Si:H layer with enough thickness enables the protection of the silicon wafer from any damage caused by bombardment during sputtering. However, due to the parasitic absorption [52] and the high resistive property [55,74], the increase of the a-Si:H layer can significantly contribute to optical and series resistance losses in solar cells. As reported by L. Tutsch et al., the MCLTs of the wafers passivated with >7-nm-thick a-Si:H(*i*) layers are almost fully restored after sputtering and after sputtering annealing, while the samples with ≤7-nm-thick passivation layers exhibit severe detrimental effects [95]. It is consistent with the thickness of a-Si:H stacks in SHJ solar cells, which lies approximately 10 nm [14].

Regarding deposition conditions, the degradation induced by ion bombardment could be suppressed by either decreasing the power applied to the targets or increasing the chamber pressure during sputtering [95]. The passivation degradation caused by ion bombardment should be correlated with either ion kinetic energy [99,100] or ion flux [86,87]. Reduction of the power leads to a decrease of the current and voltage on the target, thereby lowing both the ion flux and ion kinetic energy in the plasma deposition process [95]. On the other hand, the improvement of the chamber

pressure increases the possibility of being scattered on their way toward the substrate, which then reduces the kinetic energy and the damage of bombardment [95]. L. Tutsch et al. utilized a thin ITO film of several nanometers, which was deposited with relatively low power and high chamber pressure to protect the a-Si:H(*i*) layers-passivated Si wafer from the damage of ion bombardment [43]. As a result, the lifetime of the protected samples was improved by several folds, and their iV_{oc} was enhanced for ~26 mV in comparison with the baseline samples. The comparison of passivation degradation among different sputtering modes, including radio frequency (RF), direct current (DC), and pulsed DC modes, was summarized [84,97,98]. Due to the lower target voltage (RF: 112 V, DC: >200 V), RF sputtering exhibits less bombardment-induced damage to the passivated substrates both after sputtering and recovering after annealing.

Regardless of the damage sources in the TCO deposition process, the a-Si:H-based surface passivation can be recovered by 180−200 °C thermal annealing either during or after the deposition [87,101,102]. During the thermal treatment process, the carrier concentration at the c-Si surface (band bending) would be tuned. It was reported that the surface defects in a-Si:H passivation layers can be eliminated after annealing at 180 °C [101]. This effect is due to the transfer of hydrogen atoms from the a-Si:H(*i*) bulk toward dangling bonds at the c-Si surface, and the latter is then passivated by the formation of monohydrides. It is likely that the re-passivation of dangling bonds, caused by the sputter-induced Si−H bond rupture, follows the same principles. As reported by Demaurex et al. [86], the microstructural modification in the a-Si:H layers after sputtering and annealing was investigated by a Fourier-transform infrared spectroscopy (FTIR) measurement. In this report, the authors showed that both monohydride and multi-hydride bonds in the a-Si:H layers were descended after sputtering, while the hydride bonds recovered partially after short annealing.

3. Classification of TCO films in SHJ solar cells

Due to its superior photoelectric property and long-term stability, ITO is widely used in optoelectronic applications and has become the standard material for SHJ solar cells [1,7]. Meanwhile, the optoelectrical performance can be further improved by tuning the composition or interface modification. To reduce the use of the rare indium element, it is an attractive way to find low-cost substitutes with indium-based TCOs. AZO is a natively polycrystalline material with lower electronic quality than ITO when deposited at low temperatures (<200 °C) and as a thin layer (<100 nm), making it an attractive low-cost substitute [31,103]. Indium-based oxides [45,98,104−108] and zinc-based oxides [109−115] are the most widely studied two TCO categories in SHJ solar cells. Each of them has its limitations. In this section, we attempt to review the application of various TCOs in the field of SHJ solar cells and their performance in SHJ solar cells.

3.1. Doped indium oxides

In recent years, indium-based TCOs have attracted wide attention and been reviewed, thanks to their high conductivity to ensure the transportation of photogenerated charges as well as outstanding transparency to the sun spectrum [19]. Despite the limited indium content in the earth's crust, various cation-doped In_2O_3 have been investigated so far in SHJ solar cells [24,25]. Indium oxide doped with hydrogen, tin, tungsten, cerium, etc. are commonly used TCO materials in SHJ cells. In the following part, roadmaps toward higher efficiency by using indium-based oxides as TCOs in SHJ solar cells would be discussed.

3.1.1. ITO

Currently, more than 70% of indium is used in the production of ITO materials, which subsequently has broadly been applied as TCO films in the production of industrial SHJ solar cells [24,25]. The relatively low resistivity, high transparency, and large-scale production capability make ITO well-suited for displaying the transport channel layer on both sides in SHJ solar cells. Additionally, long-time stability and facile production are other factors to contribute ITO as the dominant TCO electrodes. Consequently, continuous improvements in industrial PCE performance have been obtained, and the breakthrough efficiency of double-side contacted SHJ solar cells reached 25.1% in 2015 [12], a world record, surpassing the champion efficiency of homojunction PERC cells (Fig. 4a). Subsequently, Kaneka Corp. published their work on IBC-SHJ (structure as Fig. 4b) with the first silicon solar cell exceeding a PCE of 26% with a FF of 83.8% [24]. Later in 2017, further progress in eliminating the parasitic absorption of a-Si:H layers by using IBC structures was reported to be a PCE of 26.7% [13]. A world-record PCE of 26.81% is achieved by LONGI Co. in 2022. However, compared with the theoretical PCE limit (close to the 28.5% theoretical ceiling predicted for a 1.1 eV band gap material), there is still a noticeable gap for the further development of ITO in SHJ solar cells in the coming years.

Most notably, the PCE of current SHJ devices is limited by the trade-off between transparency and conductivity of the TCO films. Due to the relatively low carrier mobility, which is generally below 40 $cm^2/(V•s)$, ITO films are not able to achieve high transparency and decent conductivity at the same time [1,21,24,117]. That trade-off limits the improvement of the solar cell PCE. Moreover, the strategies of pattern processing structures or multilayer reflectors have been reported that do not balance the conflicting optical and electrical properties of ITO in SHJ devices [24,117−119], but any additional layers and processes might burden the cost and complexity for the cell fabrication process. Thus, the approach for developing new TCOs with high carrier mobility and low extinction coefficient is necessary.

3.1.2. Hydrogen-doped indium oxide (IO:H)

By alternating tin in ITO materials with hydrogen to form hydrogenated indium oxide (IO:H), a high μ of 100 $cm^2/(V•s)$ has been achieved. The IO:H films exhibit extremely low solar-average absorption, coming in as one of the most ideal materials to replace ITO at the front side (Fig. 5a) [39,55,120,121−124]. By replacing the front ITO layer with IO:H, Koida et al. demonstrated a PCE of 16.1% for the SHJ solar cells [122]. A large-scale (153.4 cm^2) device with a PCE of 21.13% and a short-circuit current density (J_{sc}) of 39.18 mA/cm^2 was exhibited, showing an obvious enhancement compared to the ITO counterparts (Fig. 5b) [125]. Indeed, the incorporation of the IO:H films, instead of the conventional ITO films, enhances the J_{sc} and the resulting PCE. The detailed analysis of the solar cells revealed that the appearance of hydrogen atoms as single-charged donors and their ability to passivate defects at the grain boundaries of the polycrystalline films led to the reduction of reflection loss at the IO:H/a-Si:H interface and less optical absorption in the IO:H layers [39,120,123,124]. Compared with ITO and IZO films, the resulting IO:H films feature both high carrier mobility (with the best value of 100 $cm^2/V·s$) and large band gap values after annealing, which contribute to the J_{sc} of 39.18 mA/cm^2 [125].

Compared with the ITO materials, IO:H suffers from high contact resistance at the interface of the IO:H layer and the metal front electrode grid. This problem is avoided by inserting an ITO layer between IO:H and Ag [120]. Such IO:H/ITO bilayers have low contact resistance, low R_{sheet} as well as small free-carrier absorption, outperforming the IO:H-only or ITO-only layers in solar cells (Fig. 5c) [120]. A remarkable PCE of 22.1% for a 4-cm^2 screen-

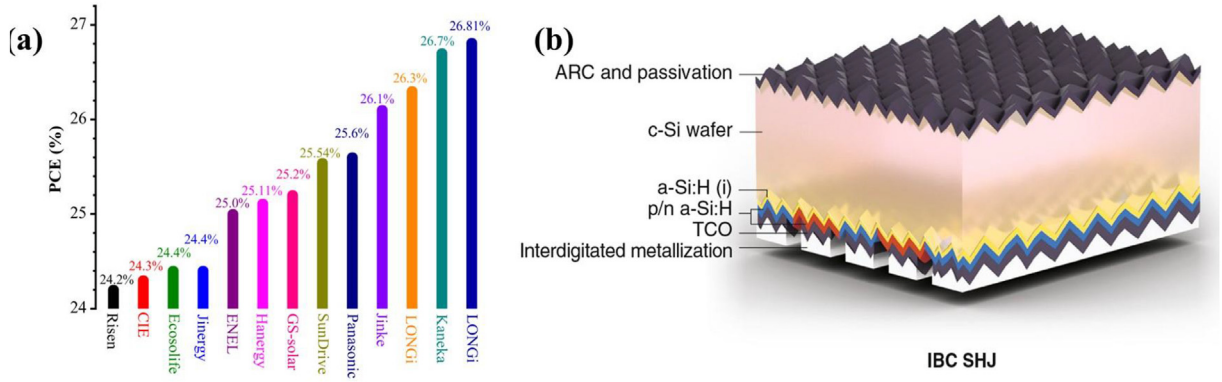

Fig. 4. (a) Champion research and development-level cell efficiencies from leading manufacturers of passivating contact technologies [24]. Copyright 2022, Elsevier. Some data are updated from the company websites. (b) The cross-sectional sketch of interdigital back-contact-silicon heterojunction [116]. Copyright 2019, Springer Nature.

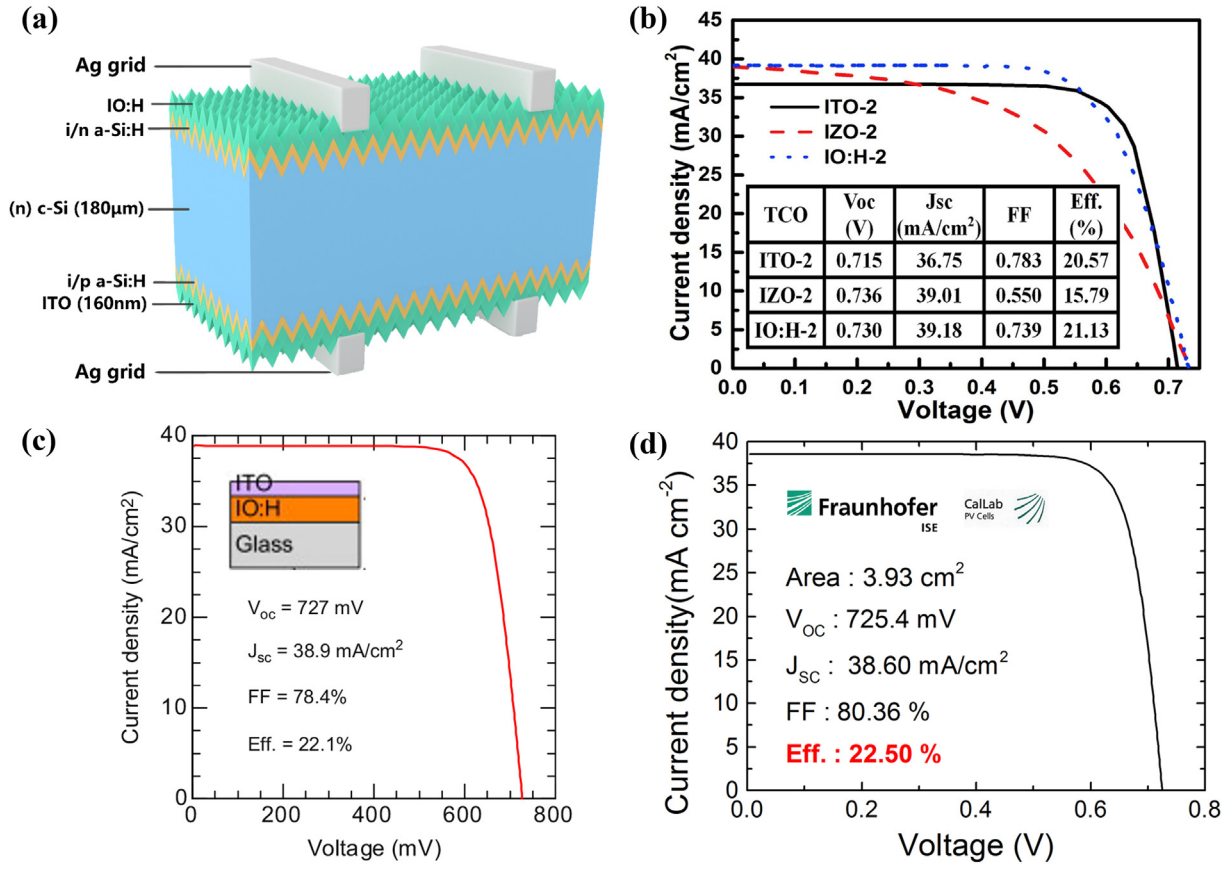

Fig. 5. (a) The schematic diagram of the structure of the IO:H-based silicon heterojunction (SHJ) solar cells. (b) the IO:H film as the front transparent conducting oxide layer showed a large-scale power conversion efficiency of 21.13% [125]. Copyright 2017, Elsevier. (c) The current density–voltage *(J-V)* characteristic of a record 4-cm^2 SHJ solar cell employing an optimized IO:H/ITO front bilayer [120]. Copyright 2013, Elsevier. (d) The light *J-V* characteristic of the IO:H-based SHJ solar cells with a Cu electrodeposited front grid (certified by the Fraunhofer ISE CalLab) [126]. Copyright 2015, The American Institute of Physics.

printed SHJ solar cell was obtained by employing an IO:H/ITO bilayer as the front transparent conductive oxide. Nevertheless, copper plating was also investigated to reduce the expensive silver usage. A certified solar cell device with a PCE of 22.5% (*FF* of 80%) is demonstrated utilizing the combination of a-Si:H/MoO_x, layers, IO:H films, and copper-plated grids (Fig. 5d) [126]. These results demonstrate that IO:H is quite an attractive alternative to ITO for SHJ solar cells.

3.1.3. Tungsten-doped indium oxide (IWO)

Tungsten-doped indium oxide (IWO), the substitution of W^{6+} for In^{3+}, is a kind of TCO film that can provide more carriers while reducing the defect concentration, compared to ITO films [127]. IWO films show high carrier mobility values of 50–80 cm^2/(V•s) [19]. Benefiting from their high electron mobility, IWO layers not only yield low resistivity but also show high NIR transmittance (94.21% at a 80 nm thickness). Moreover, there are many

fabrication methods for IWO films, beneficial for a large application. Due to the high carrier mobility, IWO materials are integrated into SHJ solar cells as transparent electrode layers on both the front and the rear sides, reducing both R_{sheet} and FCA and leading to improved performances in the solar cells (Fig. 6a). In the early stage, to obtain appropriate carrier mobility above 60 $cm^2/(V•s)$, the deposition temperature was higher than 300 °C for a long time [128]. However, this is contrary to the low process temperature requirement of SHJ solar cells. Subsequently, a series of low-temperature technologies were reported to adapt the application environment for SHJ solar cells, such as low-damage RPD or room-temperature sputtering technology [1,127–132]. Consequently, improved performances were achieved for the IWO-based SHJ solar cells to exceed 20% (Table 1). With the application of high-performance titanium and tungsten co-doped indium oxide films, large-scale SHJ solar cells (243.34 cm^2) with a high average PCE of 23.8% (with a V_{oc} of 0.746 V, a J_{sc} of 38.7 mA/cm^2 and *FF* of 82.9%) were fabricated, in which the PCE was still lower than that for the record ITO-based SHJ solar cells yet [133].

Similar to the a-Si:H/ITO interface, the a-Si:H/IWO interfacial contact is also one of the crucial factors limiting the PCEs of the SHJ solar cells. A series of strategies are applied to optimize the Schottky barrier between p-a-Si:H and IWO. One approach is to apply MgF_2 as a double-layer AR coating on top of the optimal device, the EQE-integrated J_{sc} was improved from 39.41 mA/cm^2 to 40.16 mA/cm^2 [128]. The final 8.97-cm^2 wide IWO/MgF_2-based solar cell showed an active area cell efficiency of 22.92%, which is an absolute 0.98% efficiency gain compared to the ITO counterpart, mainly due to its current gain of 1.48 mA/cm^2 (Fig. 6b, Table 1) [128]. Additionally, the H diffusion from a-Si:H to tungsten-doped indium (IWOH) is reported to not only reduce the R_{sheet} of the TCO films but also optimize the interfaces of a-Si:H/IWO [130]. The improved PCE of 22.3% for the IWOH-based solar cells was achieved on an average for 4-cm^2 SHJ cells, which have higher J_{sc} and *PCEs* than the IWO-based solar cell and similar *FF* [130]. Further, the prolonged hydrogen annealing process for the IWO-based solar cells gained the PCE by 1.14% to 23.31%, with a device area of 244.5 cm^2 [129].

The aspect of electrical and optical properties, IWO is a desirable material for industrial SHJ solar cells, especially in solar cells with low-cost copper conductor grids [138]. A SHJ solar cell with copper as the metal grids and IWO as the transparent electrodes, which are fabricated in the lab and SIMIT's R&D line, reached a PCE of over 22%, showing great potential for the copper metallization of the SHJ solar cells with reduced cost and overcoming the limitations of screen-printing technology (Fig. 6c) [131]. By now, there is a consensus within the industrialization of IWO that the content of indium in the excellent performance of IWO (In:W = 95:5) is still insufficiently ideal [128,129,137,133], where the high production costs would the pressing issue. In a word, IWO can provide advantages over ITO due to its lower absorption in the long wavelength region. However, there is still room for further improvement in conversion efficiency.

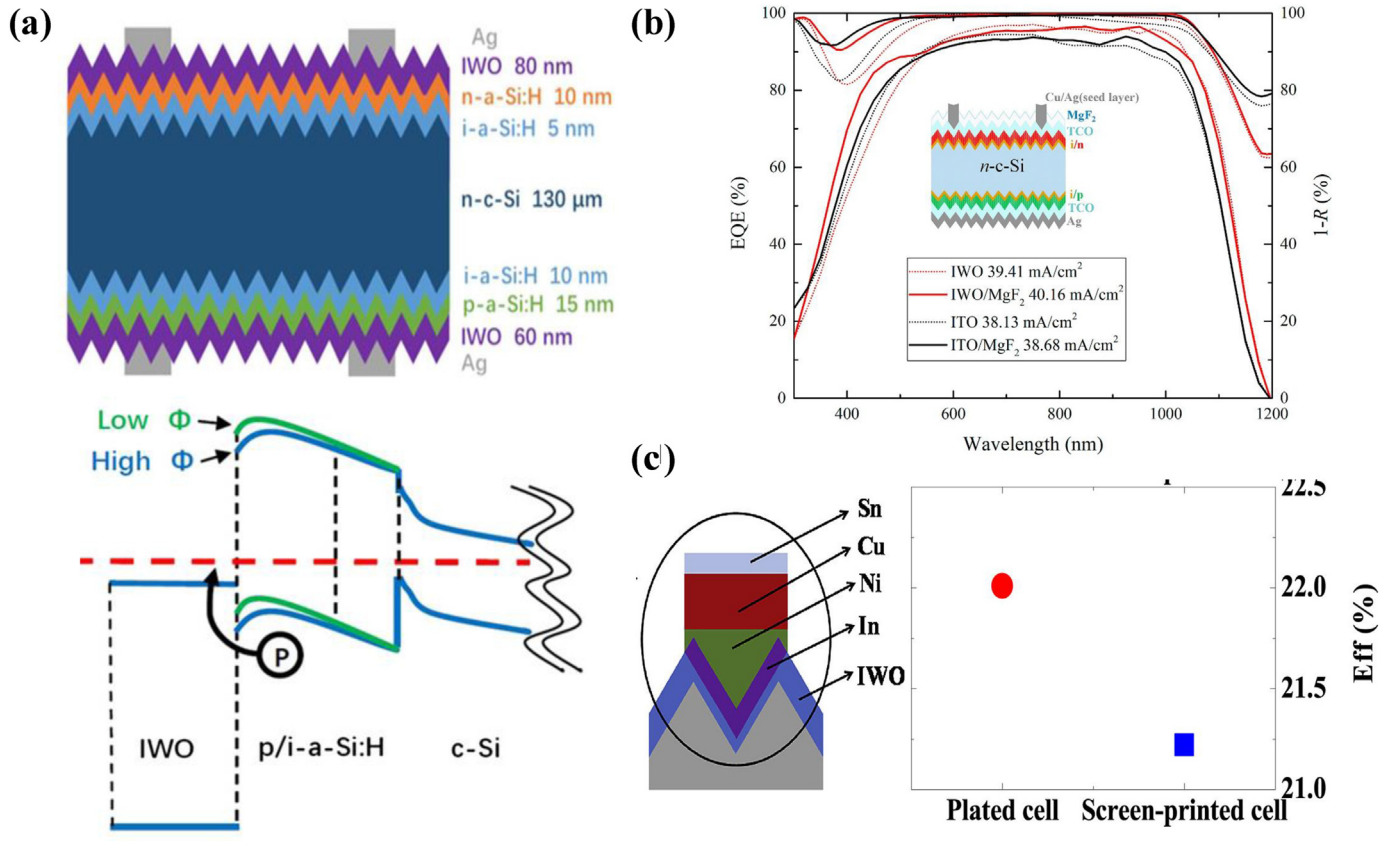

Fig. 6. (a) The architecture and band alignment of the tungsten-doped indium oxide/*p*-a-Si:H/*i*-a-Si:H/*n*-*c*-Si band alignment [129]. Copyright 2021, Wiley-VCH. (b) EQE and 1-reflection (R) of the optimal tungsten-doped indium oxide-based silicon heterojunction device and its indium tin oxide counterpart, with and without the MgF_2 top layer. The inset is the final device structure [128]. Copyright 2021, Elsevier. (c) The Sketch architecture, power conversion efficiency of a silicon heterojunction solar cell with plating Cu, and screen plating Ag contacts [131]. Copyright 2020, Elsevier.

Table 1
Summary of the representative SHJ solar cells with IWO-based TCOs.

Structure	IWO deposition method	Area (cm^2)	PCE (%)	V_{oc} (mV)	*FF* (%)	J_{sc} (mA/cm^2)	Ref.
Ag/IWO/n-a-Si:H/i-a-Si:H/n-*c*-Si/i-a-Si:H/p-a-Si:H/IWO/Ag	IP	4	22.1	723	80.4	38.1	[130]
Ag/HIWO/n-a-Si:H/i-a-Si:H/n-*c*-Si/i-a-Si:H/p-a-Si:H/HIWO/Ag	IP	4	22.3	722	80.4	38.4	[130]
Ag/IWO/n^+-a-Si:H/i-a-Si:H/n-*c*-Si/i-a-Si:H/p-a-Si:H/IWO/Ag	PRD	/	23.02	740.2	81.3	38.25	[134]
Ag/IWO/n-a-Si:H/i-a-Si:H/n-*c*-Si/i-a-Si:H/p-a-Si:H/IWO/Ag	RPD	14.6	20.8	714	76.5	38.2	[132]
Ag/IWTO/n-a-Si:H/i-a-Si:H/n-*c*-Si/i-a-Si:H/p-a-Si:H/IWTO/Ag	RPD	243.3	23.8	746	82.9	38.7	[133]
Ag/IWTO/n-a-Si:H/i-a-Si:H/n-*c*-Si/i-a-Si:H/p-a-Si:H/IWTO/Ag	RPD	244.5	23.34	724.6	84.3	38.22	[129]
Ag/IWO/MgF_2/n-a-Si:H/i-a-Si:H/n-*c*-Si/i-a-Si:H/p-a-Si:H/MgF_2/IWO/Ag	RF	8.97	22.92	/	/	40.16	[128]
Cu/IWO/n-a-Si:H/i-a-Si:H/n-*c*-Si/i-a-Si:H/p-a-Si:H/IWO/Cu	RPD	/	22.03	727.8	78.5	38.56	[135]
Sn/Cu/Ni/In/IWO/n^+-a-Si:H/i-a-Si:H/n-*c*-Si/i-a-Si:H/p-a-Si:H/IWO/In/Ni/Cu/Sn	RPD	/	22.01	/	78.8	/	[131]
Cu/IWO/n^+-a-Si:H/i-a-Si:H/n-*c*-Si/i-a-Si:H/p-a-Si:H/IWO/Cu	RPD	/	22	728.1	77.8	38.82	[136]
Ag/IWO/n-a-Si:H/i-a-Si:H/n-*c*-Si/i-a-Si:H/p-a-Si:H/IWO/Ag	RPD	244.6	25.18	744.3	86.9	/	[137]

Abbreviations: RPD, reactive plasma deposition; RF, radio frequency; IWO, tungsten-doped indium oxide; PCE, power conversion efficiency; FF, fill factor; SHJ, silicon heterojunction.

3.1.4. Alternative doped indium oxide

To date, there are indium-based TCOs with other doping metals such as cerium, titanium, and zirconium, which mainly perform as front transparent electrodes for the solar cells having sensitivity in the visible to the NIR wavelength region [78,125,139–141]. The large potential of the optimally processed In_2O_3:Ce:H (ICO:H) window layers in SHJ cells is demonstrated, quantified by the improvement in J_{sc} of 0.6 mA/cm^2 without impairing the resistive losses in comparison to the usage of baseline ITO layers [139]. By further incorporating ICO:H instead of conventional ITO and IO:H films, an improved PCE of 24.1%, a V_{oc} of 745 mV, a J_{sc} of 38.8 mA/cm^2, and a *FF* of 83.2% were obtained [78]. It is believed that their high carrier mobility of 140 $cm^2/(V \cdot s)$ contributed to their high efficiency. Already, SHJ solar cells with the optimized indium zirconium oxide (IZrO) front electrodes resulted in a J_{sc} of 40 mA/cm^2, a *FF* of 80%, and a PCE of 23.4% [141]. A heterojunction solar cell with an ITO/IZrO bilayer electrode succeeds in a J_{sc} of 38.72 mA/cm^2, a *FF* of 82.39%, and a PCE of up to 23.59% [140]. Similarly, the significant reduction of the reflection loss of the conventional and needle-like Hf-doped In_2O_3 (IHFO) bilayer films deposited on the textured silicon was observed. The short-circuit current and efficiency of the solar cell were improved by 0.52 mA/cm^2 and 0.39%, utilizing a needle-like IHFO thin film as an AR layer [134].

As for the manufacturing capacity of SHJ solar cells increases or future tandem devices, there are significant concerns about the use of indium. The values of indium consumption per cell and per generated power for SHJ solar cells from different sources exhibited large discrepancies, but all available data indicate concern about the insufficient supply of indium to support in the future [25]. Significantly, reducing indium consumption for TCO films has become mandatory to push SHJ solar cell technology toward a terawatt scale production due to material scarcity and costs. As an alternative to minimizing the use of metallic indium, thin indium-based TCOs (with better performance) or the IBC cell design might be a choice. With a reduced thickness of approximately 30 nm for ITO layers, the resource-sustainable manufacturing capacity of SHJ solar cells would be substantially increased to 115–330 GW. However, this would only account for approximately 5–10% of a 3 TW market size, suggesting that the SHJ solar cell using ITO in some form remains a niche product. Moreover, reducing the thickness of ITO layers could also lead to significant increases in ρ_c due to the changes in current pathways and the current crowding effect. For example, 20-nm-thick ITO capped by a non-indium-based TCO would greatly increase the sustainable manufacturing capacity compared to the present implementation for SHJ solar cells relying solely on ITO [25]. Thus, substituting part or full of ITO with a more transparent and less expensive dielectric indium-free film is promising.

3.2. Doped zinc oxide

Typically, an approximately 70-nm-thick ITO layer is used on each surface to form thin transparent conductive layers at the front and rear of the SHJ solar cells, corresponding to approximately 5.7 mg/W consumption of ITO and 4.2 mg/W consumption of indium, with an assumed cell PCE of 25.11% [25]. Thus, the future of c-Si PVs would benefit greatly from any alternative indium-free layer to circumvent the parasitic absorption in TCOs. As for the choice of indium-free TCOs in SHJ, AZOs, with low cost, abundant material reserves in nature and capability of achieving comparable efficiencies to the ITO-based SHJ solar cells, has been considered as one of the few potential alternatives to ITOs [109,142].

To reduce the use of indium, both ITO 50%/AZO 50% and ITO 25%/AZO 50%/ITO 25% were used on the back of SHJ solar cells with a decent performance, which was close to that of individual ITO (Fig. 7a) [114]. The performance of the SHJ solar cells with such two kinds of TCO stacks as the back TCO layers was greatly improved compared to that with the individual AZO layer [114]. Meanwhile, the PCE gap between such the ITO/AZO stacks and the individual ITO stack could be narrowed to approximately 0.1% (absolute value), showing the possibility of applying the ITO/AZO stack structure in the SHJ solar cell [114].

Considering the use of indium-free TCOs, the AZO layers were used in three different cell configurations labeled as 'front-AZO cell', 'back-AZO cell'. and 'all-AZO cell' [144]. At the early stage, it was found that the PCE was challenging to exceed 20% for the SHJ solar cells with the direct application of the individual AZO film as a front-AZO cell (Table 2) [109,142]. For further improving the light coupling by textured AZO or the implementation of the electrochemically grown ZnO nanorod as AR layers on AZO, less discernible enhancement of the PCE was observed (Fig. 7b) [142]. Thanks to the optimization of experimental conditions for AZO, the above-mentioned front AZO cell showed an overall increasing PCE of over 20% [143]. The low PCE was attributed to the poor contact of a-Si:H(*p*)/AZO and the low electrical and optical properties of AZO. The optimized low-resistivity a-Si:H(*p*)/AZO contact by the implementation of a trimethyl boron ($B(CH_3)_3$) doped a-Si:H(*p*) film as a hole transport layer enables a *FF* above 81% and a PCE of 23.6% for the front-AZO SHJ solar cells, comparable with 23.7%-efficient cells using traditional ITO (Fig. 7c) [143]. In addition, the back-AZO cell experienced a similar performance improvement path as that of the front-AZO cell. Featuring a standard screen-printed silver grid at the front with approximately 3.25% optical shadowing, a champion device of the black-AZO cell a J_{sc} of up to 40.81 mA/cm^2 and a PCE of 23.96% was obtained [112]. As for all-AZO cells, a 4-cm^2 cell was certified at ISFH CalTec with an efficiency of 23.0%, a V_{OC} of 738.8 mV, a *FF* of 80.3%, and a J_{SC} of 38.7 mA/cm^2 [145].

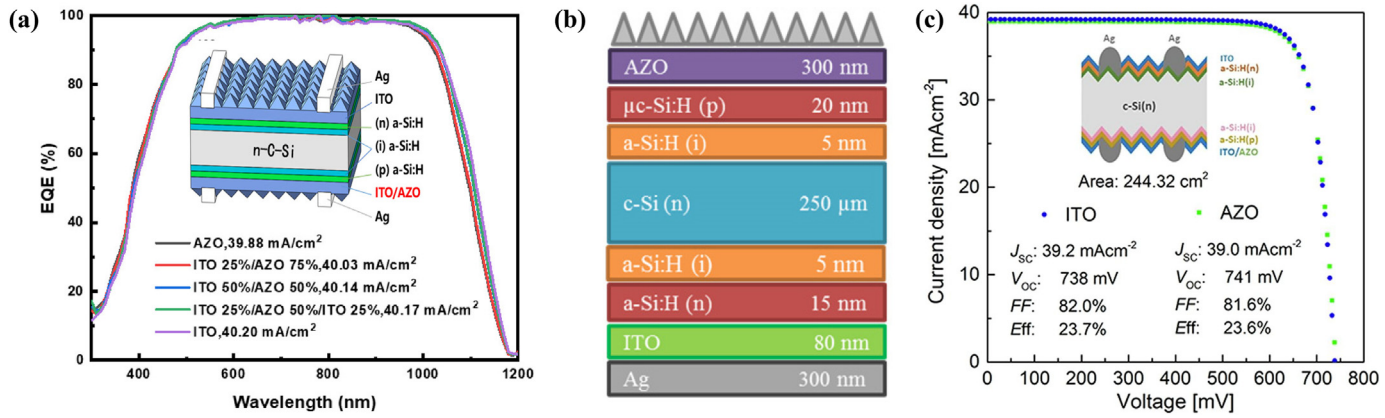

Fig. 7. (a) EQE of the silicon heterojunction (SHJ) solar cell as a function of the indium tin oxide / aluminum-doped zinc oxide (AZO) thickness fraction [114]. Copyright 2021, American Chemical Society. (b) The *J-V* curves of the illuminated SHJ solar cells (Al/AZO/a-Si:H(*n*)/a-Si:H(*i*)/c-Si(*p*)/Al) before and after the hydrogen plasma treatment on the front AZO layer [142]. Copyright 2016, Elsevier. (c) The *J-V* characteristic of the SHJ cells with indium tin oxide or AZO as the rear side transparent conducting oxide film [143]. Copyright 2021, Elsevier.

Table 2
Summary of the representative SHJ solar cells with AZO as part of the TCO layers.

Device structure	TCO deposition method	Area (cm^2)	PCE (%)	V_{oc} (mV)	*FF* (%)	J_{sc} (mA/cm^2)	Ref.
Ag/ITO/n-a-Si:H/i-a-Si:H/n-*c*-Si/i-a-Si:H/p-a-Si:H/ITO(25%)/AZO(50%)/ITO(25%)/Ag	DC magnetron sputtering	245.7	/	/	/	40.17	[114]
Al/n-a-Si:H/i-a-Si:H/n-*c*-Si/i-a-Si:H/p-a-Si:H/AZO/Al	Pulsed DC magnetron sputtering	0.253	6.97	470	68	21.82	[115]
Al/AZO/a-Si:H(n)/a-Si:H(i)/c-Si(p)/Al	RF magnetron sputtering	/	13.5	590	71.2	32.1	[109]
Ag/ITO/n-a-Si:H/i-a-Si:H/n-*c*-Si/i-a-Si:H/p-a-i-Si:H/AZO/Ag/ZnO nanorods	DC magnetron sputtering	/	14.9	652.9	75.2	30.3	[142]
Ag/ITO/n-a-Si:H/i-a-Si:H/n-*c*-Si/i-a-Si:H/p-a-Si:H/AZO/Ag	Sputtering	/	23.6	741	81.6	39.0	[143]
Ag/AZO/n-a-Si:H/i-a-Si:H/n-*c*-Si/i-a-Si:H/p-a-Si:H/ITO/Ag	RF magnetron sputtering	4	23.96	726	80.87	40.81	[112]

Abbreviations: RF, radio frequency; DC, direct current; AZO, aluminum-doped zinc oxide; TCO, transparent conducting oxide; PCE, power conversion efficiency; FF, fill factor; SHJ, silicon heterojunction.

Furthermore, an all-AZO cell with a 244 cm^2 total area reached a PCE as high as 21.3% by using an amorphous silicon oxide layer (a-SiO_2) as an AR coating. Thus far, AZO appeared to be a promising indium-free alternative material to replace the back ITO commonly used in SHJ solar cells.

Remarkably, the environmental stability of AZO films is still an unsolved problem [113,145]. Significantly increasing electrical resistivity and surface degradation were obtained, when the AZO is exposed to a harsh environment (e.g. annealing in the air or humidity damping). Damp heat test results of encapsulated SHJ devices with AZO as the TCO films exhibited relative *FF* degradation of 7% after 1000 h [145]. This drawback prevents AZO films to be deployed in real applications that require long-term reliability of the devices. Thus, a significant amount of effort still needs to be put into battle with the relatively poor conductivity and long-term stability of AZO layers. For example, the *FF* degradation rate might reduce with the deposition of a-SiO_2 or SiN_x under humid conditions [145]. However, it is still an open question whether a TCO-free design could potentially give optimal device performance.

3.3. Other TCOs

Alternatively, silver nanowires (Ag NWs) and graphene have also attracted attention [146–151]. Ag NWselectrodes can be deposited on top of the SHJ structure by mechanical transfer or solution technologies while achieving excellent transmittance and conductivity. However, Ag was reported to maintain low contact resistance between the silicon layer and metal, but it could easily react with a thin-film silicon layer to form an insulating layer of AgO that blocks charge extraction. The issues remain to be tackled in the other metal-based TCOs, such as Ti, Cu, et al. [23] By inserting a SiN_x layer to suppress the deterioration of the passivation quality of the Ti layer induced by direct metal-to-a-Si:H contacts, an indium-free design for SHJ solar cells achieve low series resistivity, a decent *FF* (80.7%), and efficiencies (>22%) [118]. Regarding graphene-based TCOs, until now, it is still arguable for use as a transparent electrode for any solar cell, since it would absorb significantly over the full spectrum and shows large R_{sheet} [147].

4. TCO films for practical applications

In mass production, rear-emitter (RE) structures (metal/TCO/a-Si:H(p)/a-Si:H(i)/c-Si(n)/a-Si:H(i)/a-Si:H(n)/TCO/metal) are nowadays widely applied in the mass production of SHJ solar cells, taking the place of the traditional front emitter structures (metal/TCO/a-Si:H(n)/a-Si:H(i)/c-Si(n)/a-Si:H(i)/a-Si:H(p)/TCO/metal) [7,14,152]. As discussed above , it is a trade-off between lateral conductivity and transparency in TCO films. And in RE structures, by alternating the p/n junction with the high/low junction [32,152,153] at the front side, the lateral transport of the free carriers partially shifted from the TCO films into the Si wafer, slightly decreasing the R_{sheet}. As a result, the trade-off between optical and electrical properties becomes less stringent at the front side [119,153]. Therefore, the requirements of the TCO films for the front and the rear sides are different, depending on the structures of the SHJ solar cells. In RE structures, the requirement of the front side TCO films is primarily on their optical properties rather than their electrical ones, which means low absorption and high carrier mobility but relatively low

carrier density. While the rear side needs better electron properties like relatively high carrier density and high carrier mobility.

ITO materials have been widely applied as transparent electrodes, ever since the beginning of the SHJ solar cell development. It has been proven that the ratio of In:Sn played an important role in manipulating the carrier density, mobility, and transmittance of the ITO films [59]. In SHJ solar cell mass production, 97/3-ITO films (mass ratio of $In_2O_3/SnO_2 = 97/3$) are chosen as the front TCO layers due to their excellent transparent capacity [154]. While 90/10-ITO films (mass ratio of $In_2O_3/SnO_2 = 90/10$) are integrated on the rear sides because of their low resistance [154]. With the improvement of PCEs of the SHJ solar cells, the relatively low carrier mobility of the ITO materials of less than 40 cm/(V·s) is gradually becoming a limiting factor, especially on the front side. Therefore, to improve the PCE of the SHJ solar cells, TCO materials with excellent transparency and high carrier mobility are introduced into the cells. Dong et al. [14]. selected a multidoped indium-based material IMO:H to enhance the charge mobility of the front TCO films, and a certified PCE of 25.26% is accomplished. The IMO:H layers exhibited high carrier mobility of over 70 cm/(V·s) at a N_e of around 2×10^{20} cm^{-3} and improved transmittance within below the 400-nm-wavelength range. Additionally, the IMO: H films were also proven to possess lower ρ_c with μc-Si:H(n).

Besides the PCEs, the total cost of SHJ solar cell is also a critical obstacle to industrialization. Benefiting the uniquely indispensable TCO layers in SHJ, a low-temperature—sintering metal paste could be used, providing the possibility to reduce the cost by using scarce materials. Silver in the grid electrodes is going to be reduced or replaced by a base metal, such as Cu@Ag core-shell materials [155] or Cu with surface oxidation resistance [156]. Until 2021, the costs of TCO targets are still an important factor, which spend more than 10% of the consumable costs [7]. The main reason is the relatively high price of indium [26]. Hence, indium-free TCO materials, such as AZO [112,145], are also attempted to integrate into the SHJ solar cells. Compared with ITO, stability verified by industry and academia, it is still an open question whether a TCO-free design could potentially give optimal device performance since the environmental stability of AZO films is still an unsolved issue. AZO films still face challenges of relatively high resistivity [157,158]. Another possible approach would be using multilayered AR coatings such as SiO_x [24], SiN_x [118,119], and MgF_2 [117] on top of extremely thin ITO layers. In this way, the usage of indium could be reduced while still maintaining low resistivity contact. For example, SHJ solar cells have the potential to achieve an excellent J_{sc} beyond 42 mA/cm^2 if the front-side ITO layer can be replaced by an ITO/SiN_x double layer [118,119].

5. Summary and perspective

Herein, we presented a comprehensive review covering all the aspects of TCO films in the application of SHJ solar cells, from basic functions to materials, as well as their application in mass production. SHJ solar cells are a fundamental approach for accomplishing high-efficiency PV devices. In SHJ solar cells, the TCO films act as literal conductive layers which connect the doped a-/μc-Si:H layers and the metal grids. As a fundamental role in the solar cells, the TCO films have a key impact on PCEs and the production cost of the solar cell intensively. ITO materials are still the most widely applied TCOs in SHJ solar cells in mass production. But their relatively low carrier mobility of less than 40 cm/(V•s) is becoming a limiting factor to meet the continuous demand for elevating solar cell performance. Meanwhile, the high indium consumption of ITO films hinders further reducing the production cost. Therefore, TCO materials, deposition techniques as well as PVD equipment should be further investigated for SHJ solar cells to enhance the performance and mitigate the cost. Here, we outline possible research approaches and challenges that have to be addressed for the future development of TCO films.

Development of high-mobility TCOs. In TCO films, it is a trade-off between the conductivity and the transparency *via* tuning N_e. While with the improvement of μ, the conductivity of TCO films could be enhanced without any losses in transmittance. Hence, the development of high-mobility (>100 cm^2/(V•s)) TCO materials is highly required for the mass production of SHJ solar cells.

Application of multilayered TCO structures. To deduct the ρ_c of the TCO/doped *a*-Si:H and the TCO/Ag grid interfaces, the materials composite from the front to the rear side of TCO films should be different. Consequently, multilayer structures, in which materials with different WFs or N_e, should be applied in TCO films.

Low-damage TCO coating methods. The PVD coating methods and processes to fabricate TCO films play a significant role on the passivation effect of the substrates. Therefore, the development of low-damage TCO coating equipment or processes that are suitable for mass production is indispensable for improving cell efficiency.

Reduction of indium consumption. The high indium consumption of TCO films is one of the detrimental factors that hinders the cost reduction of SHJ solar cells. To deduct the indium consumption or develop indium-free TCO films, it is highly required to apply in SHJ solar cells. Meanwhile, the technique of deposition of an ARC on top of the TCO films, which means shrinking the thickness of TCO films, also should be applied in solar cells.

Silicon solar cells can be manufactured, even at the TW scale, where the photoactive bulk silicon layer avoids any scarce materials, and the silver grid electrode is going to be substituted by base metals, such as copper. SHJ solar cells are going to be the predominant production in the market of Si-based PV devices in the future. As the key cost issues for the SHJ devices, the development of TCO films still faces some challenges. We believe this review would prompt us to learn the achievements, remaining challenges, as well as possible investigation directions, and promote the development of TCO films in SHJ solar cells rapidly.

Declaration of competing interest

The authors declare that they have no known competing financial interests or personal relationships that could have appeared to influence the work reported in this paper.

Data availability

Data will be made available on request.

Acknowledgments

This work was supported by the Jiangsu Provincial Departments of Science and Technology (BE2022025), the Natural Science Foundation of China (No. 62274116), China Postdoctoral Science Foundation (No. 2020M681703), the Priority Academic Program Development of Jiangsu Higher Education Institutions, the 111 Program, and Collaborative Innovation Center of Suzhou Nano Science and Technology (NANO—CIC).

References

[1] Y. Liu, Y. Li, Y. Wu, G. Yang, L. Mazzarella, P. Procel-Moya, A.C. Tamboli, K. Weber, M. Boccard, O. Isabella, X. Yang, B. Sun, High-efficiency silicon heterojunction solar cells: materials, devices and applications, Mater. Sci. Eng. R 142 (2020), 100579, https://doi.org/10.1016/j.mser.2020.100579.

[2] M. Fischer, M. Woodhouse, S. Herritsch, J. Trube, International Technology Roadmap for Photovoltaic (ITRPV), Thirteenth ed., VDMA e.V., Frankfurt, Germany, 2022. https://itrpv.vdma.org/.

[3] M. Hermle, F. Feldmann, M. Bivour, J.C. Goldschmidt, S.W. Glunz, Passivating contacts and tandem concepts: approaches for the highest silicon-based solar cell efficiencies, Appl. Phys. Rev. 7 (2020), 021305, https://doi.org/10.1063/1.5139202.

[4] JinkoSolar Achieves 26.4% Conversion Efficiency For 182mm High-Efficiency N-Type TOPCon Monocrystalline Silicon Cell, 2022. https://taiyangnews.info/technology/26-4-efficiency-for-n-type-monocrystalline-silicon-solar-cell/.

[5] F. Fertig, R. Lantzsch, A. Mohr, M. Schaper, M. Bartzsch, D. Wissen, F. Kersten, A. Mette, S. Peters, A. Eidner, J. Cieslak, K. Duncker, M. Junghänel, E. Jarzembowski, M. Kauert, B. Faulwetter-Quandt, D. Meißner, B. Reiche, S. Geißler, S. Hörnlein, C. Klenke, L. Niebergall, A. Schönmann, A. Weihrauch, F. Stenzel, A. Hofmann, T. Rudolph, A. Schwabedissen, M. Gundermann, M. Fischer, J.W. Müller, D.J.W. Jeong, Mass production of p-type Cz silicon solar cells approaching average stable conversion efficiencies of 22, Energy Proc. 124 (2017) 338–345, https://doi.org/10.1016/j.egypro.2017.09.308.

[6] M.A. Green, E.D. Dunlop, G. Siefer, M. Yoshita, N. Kopidakis, K. Bothe, X. Hao, Solar cell efficiency tables (version 61), Prog. Photovolt. Res. Appl. 31 (2023) 3–16, https://doi.org/10.1002/pip.3646.

[7] Z. Sun, X. Chen, Y. He, J. Li, J. Wang, H. Yan, Y. Zhang, Toward efficiency limits of crystalline silicon solar cells: recent progress in high-efficiency silicon heterojunction solar cells, Adv. Energy Mater. 12 (2022), 2200015, https://doi.org/10.1002/aenm.202200015.

[8] M. Taguchi, M. Tanaka, T. Matsuyama, T. Matsuoka, S. Tsuda, S. Nakano, Y. Kishi, Y. Kuwano, Improvement of the conversion efficiency of polycrystalline silicon thin film solar cell, in: Proceedings of the 5th European Photovoltaic Solar Energy Conference, 1990, pp. 689–692.

[9] M. Taguchi, Y. Tsunomura, H. Inoue, S. Taira, T. Nakashima, T. Baba, H. Sakata, E. Maruyama, High efficiency HIT solar cell on thin (<100 μm) silicon wafer, in: Proceedings of the 24th European Photovoltaic Solar Energy Conference, 2009, pp. 1690–1693.

[10] T. Kinoshita, D. Fujishima, A. Yano, A. Ogane, S. Tohoda, K. Matsuyama, Y. Nakamura, N. Tokuoka, H. Kanno, H. Sakata, M. Taguchi, E. Maruyama, The Approaches for High Efficiency HITTM Solar Cell with Very Thin (<100 Micrometre) Silicon Wafer over 23 Percent, 26th European Photovoltaics Solar Energy Conference and Exhibition Proceedings, 2011, pp. 871–874.

[11] M. Taguchi, A. Yano, S. Tohoda, K. Matsuyama, Y. Nakamura, T. Nishiwaki, K. Fujita, E. Maruyama, 24.7% record efficiency HIT solar cell on thin silicon wafer, IEEE J. Photovolt. 4 (2014) 96–99, https://doi.org/10.1109/JPHOTOV.2013.2282737.

[12] D. Adachi, J.L. Hernández, K. Yamamoto, Impact of carrier recombination on fill factor for large area heterojunction crystalline silicon solar cell with 25.1% efficiency, Appl. Phys. Lett. 107 (2015), 233506, https://doi.org/10.1063/1.4937224.

[13] K. Yoshikawa, H. Kawasaki, W. Yoshida, T. Irie, K. Konishi, K. Nakano, T. Uto, D. Adachi, M. Kanematsu, H. Uzu, K. Yamamoto, Silicon heterojunction solar cell with interdigitated back contacts for a photoconversion efficiency over 26%, Nat. Energy 2 (2017), 17032 https://doi.org/10.1038/nenergy.2017.32.

[14] G. Dong, J. Sang, C.-W. Peng, F. Liu, Y. Zhou, C. Yu, Power conversion efficiency of 25.26% for silicon heterojunction solar cell with transition metal element doped indium oxide transparent conductive film as front electrode, Prog. Photovolt. Res. Appl. 30 (2022) 1136–1143, https://doi.org/10.1002/pip.3565.

[15] At 26.81%, LONGi Sets a New World Record Efficiency for Silicon Solar Cells, 2022. https://www.longi.com/en/news/propelling-the-transformation/.

[16] W. Shockley, H.J. Queisser, Detailed balance limit of efficiency of p-n junction solar cells, J. Appl. Phys. 32 (1961) 510–519, https://doi.org/10.1063/1.1736034.

[17] M. Anaya, G. Lozano, M.E. Calvo, H. Míguez, ABX_3 perovskites for tandem solar cells, Joule 1 (2017) 769–792, https://doi.org/10.1016/j.joule.2017.09.017.

[18] M. De Bastiani, A.S. Subbiah, E. Aydin, F.H. Isikgor, T.G. Allen, S. De Wolf, Recombination junctions for efficient monolithic perovskite-based tandem solar cells: physical principles, properties, processing and prospects, Mater. Horiz. 7 (2020) 2791–2809, https://doi.org/10.1039/D0MH00990C.

[19] G.K. Dalapati, H. Sharma, A. Guchhait, N. Chakrabarty, P. Bamola, Q. Liu, G. Saianand, A.M. Sai Krishna, S. Mukhopadhyay, A. Dey, T.K.S. Wong, S. Zhuk, S. Ghosh, S. Chakrabortty, C. Mahata, S. Biring, A. Kumar, C.S. Ribeiro, S. Ramakrishna, A.K. Chakraborty, S. Krishnamurthy, P. Sonar, M. Sharma, Tin oxide for optoelectronic, photovoltaic and energy storage devices: a review, J. Mater. Chem. 9 (2021) 16621–16684, https://doi.org/10.1039/D1TA01291F.

[20] J. Huang, Z. Yin, Q. Zheng, Applications of ZnO in organic and hybrid solar cells, Energy Environ. Sci. 4 (2011) 3861–3877, https://doi.org/10.1039/c1ee01873f.

[21] D.A. Jacobs, M. Langenhorst, F. Sahli, B.S. Richards, T.P. White, C. Ballif, K.R. Catchpole, U.W. Paetzold, Light management: a key concept in high-efficiency perovskite/silicon tandem photovoltaics, J. Phys. Chem. Lett. 10 (2019) 3159–3170, https://doi.org/10.1021/acs.jpclett.8b03721.

[22] Y. Xu, J. Wang, L. Sun, H. Huang, J. Han, H. Huang, L. Zhai, C. Zou, Top transparent electrodes for fabricating semitransparent organic and perovskite solar cells, J. Mater. Chem. C 9 (2021) 9102–9123, https://doi.org/10.1039/d1tc02413b.

[23] C. Han, R. Santbergen, M. van Duffelen, P. Procel, Y. Zhao, G. Yang, X. Zhang, M. Zeman, L. Mazzarella, O. Isabella, Towards bifacial silicon heterojunction solar cells with reduced TCO use, Prog. Photovolt. Res. Appl. 30 (2022) 750–762, https://doi.org/10.1002/pip.3550.

[24] A. Razzaq, T.G. Allen, W. Liu, Z. Liu, S. De Wolf, Silicon heterojunction solar cells: techno-economic assessment and opportunities, Joule 6 (2022) 514–542, https://doi.org/10.1016/j.joule.2022.02.009.

[25] Y. Zhang, M. Kim, L. Wang, P. Verlinden, B. Hallam, Design considerations for multi-terawatt scale manufacturing of existing and future photovoltaic technologies: challenges and opportunities related to silver, indium and bismuth consumption, Energy Environ. Sci. 14 (2021) 5587–5610, https://doi.org/10.1039/D1EE01814K.

[26] J. Haschke, O. Dupré, M. Boccard, C. Ballif, Silicon heterojunction solar cells: recent technological development and practical aspects – from lab to industry, Sol. Energy Mater. Sol. Cells 187 (2018) 140–153, https://doi.org/10.1016/j.solmat.2018.07.018.

[27] S.D. Wolf, A. Descoeudres, Z.C. Holman, C. Ballif, High-efficiency silicon heterojunction solar cells: a review, Green 2 (2012) 7–24, https://doi.org/10.1515/green-2011-0018.

[28] B.K. Ghosh, C.N.J. Weoi, A. Islam, S.K. Ghosh, Recent progress in Si heterojunction solar cell: a comprehensive review, Renew. Sustain. Energy Rev. 82 (2018) 1990–2004, https://doi.org/10.1016/j.rser.2017.07.022.

[29] C. Ballif, F.-J. Haug, M. Boccard, P.J. Verlinden, G. Hahn, Status and perspectives of crystalline silicon photovoltaics in research and industry, Nat. Rev. Mater. 7 (2022) 597–616, https://doi.org/10.1038/s41578-022-00423-2.

[30] K. Ellmer, Past achievements and future challenges in the development of optically transparent electrodes, Nat. Photon. 6 (2012) 809–817, https://doi.org/10.1038/nphoton.2012.282.

[31] Y. Chen, Review of ZnO transparent conducting oxides for solar applications, IOP Conf. Ser. Mater. Sci. Eng. 423 (2018), 012170, https://doi.org/10.1088/1757-899x/423/1/012170.

[32] H. Park, Y.J. Lee, J. Park, Y. Kim, J. Yi, Y. Lee, S. Kim, C.K. Park, K.J. Lim, Front and back TCO research review of a-Si/c-Si heterojunction with intrinsic thin layer (HIT) solar cell, Trans. Electr. Electron. Mater. 19 (2018) 165–172, https://doi.org/10.1007/s42341-018-0026-8.

[33] F. Ruske, Deposition and properties of TCOs, in: W.G.J.H.M. van Sark, L. Korte, F. Roca (Eds.), Physics and Technology of Amorphous-Crystalline Heterostructure Silicon Solar Cells, Springer Berlin Heidelberg, Berlin, Heidelberg, 2012, pp. 301–330.

[34] E. Fortunato, D. Ginley, H. Hosono, D.C. Paine, Transparent conducting oxides for photovoltaics, MRS Bull. 32 (2011) 242–247, https://doi.org/10.1557/mrs2007.29.

[35] K. Ellmer, R. Mientus, Carrier transport in polycrystalline transparent conductive oxides: a comparative study of zinc oxide and indium oxide, Thin Solid Films 516 (2008) 4620–4627, https://doi.org/10.1016/j.tsf.2007.05.084.

[36] A. Klein, C. Körber, A. Wachau, F. Säuberlich, Y. Gassenbauer, S.P. Harvey, D.E. Proffit, T.O. Mason, Transparent conducting oxides for photovoltaics: manipulation of fermi level, work function and energy band alignment, Materials 3 (2010) 4892–4914, https://doi.org/10.3390/ma3114892.

[37] T. Minami, T. Miyata, T. Yamamoto, Work function of transparent conducting multicomponent oxide thin films prepared by magnetron sputtering, Surf. Coat. Technol. 108–109 (1998) 583–587, https://doi.org/10.1016/S0257-8972(98)00592-1.

[38] S.J. Pearton, D.P. Norton, K. Ip, Y.W. Heo, T. Steiner, Recent advances in processing of ZnO, J. Vac. Sci. Technol. B 22 (2004) 932–948, https://doi.org/10.1116/1.1714985.

[39] B. Macco, Y. Wu, D. Vanhemel, W.M.M. Kessels, High mobility In_2O_3:H transparent conductive oxides prepared by atomic layer deposition and solid phase crystallization, Phys. Status Solidi RRL 8 (2014) 987–990, https://doi.org/10.1002/pssr.201409426.

[40] R.J. Mendelsberg, G. Garcia, D.J. Milliron, Extracting reliable electronic properties from transmission spectra of indium tin oxide thin films and nanocrystal films by careful application of the Drude theory, J. Appl. Phys. 111 (2012), 063515, https://doi.org/10.1063/1.3695996.

[41] L. Tutsch, Implementing Sputter-Deposited Transparent Conductive Metal Oxides into Passivating Contacts for Silicon Solar Cells, Universität Freiburg, 2020. Dissertation.

[42] S. Calnan, A.N. Tiwari, High mobility transparent conducting oxides for thin film solar cells, Thin Solid Films 518 (2010) 1839–1849, https://doi.org/10.1016/j.tsf.2009.09.044.

[43] L. Tutsch, M. Bivour, W. Wolke, M. Hermle, J. Rentsch, Influence of the transparent electrode sputtering process on the interface passivation quality of silicon heterojunction solar cells, in: Proceedings of the 33rd European PV Solar Energy Conference and Exhibition, 2017, pp. 24–29.

[44] R. Mientus, K. Ellmer, Reactive magnetron sputtering of tin-doped indium oxide (ITO): influence of argon pressure and plasma excitation mode, Surf. Coat. Technol. 142–144 (2001) 748–754, https://doi.org/10.1016/S0257-8972(01)01160-4.

[45] A. Chen, K. Zhu, H. Zhong, Q. Shao, G. Ge, A new investigation of oxygen flow influence on ITO thin films by magnetron sputtering, Sol. Energy Mater. Sol. Cells 120 (2014) 157–162, https://doi.org/10.1016/j.solmat.2013.08.036.

[46] H.-N. Cui, V. Teixeira, L.-J. Meng, R. Martins, E. Fortunato, Influence of oxygen/argon pressure ratio on the morphology, optical and electrical properties of ITO thin films deposited at room temperature, Vacuum 82 (2008) 1507–1511, https://doi.org/10.1016/j.vacuum.2008.03.061.

[47] L. Kerkache, A. Layadi, A. Mosser, Effect of oxygen partial pressure on the structural and optical properties of dc sputtered ITO thin films, J. Alloys Compd. 485 (2009) 46–50, https://doi.org/10.1016/j.jallcom.2009.06.103.

[48] J. Wang, C. Meng, L. Zhao, W. Wang, X. Xu, Y. Zhang, H. Yan, Effect of residual water vapor on the performance of indium tin oxide film and silicon heterojunction solar cell, Sol. Energy 204 (2020) 720–725, https://doi.org/10.1016/j.solener.2020.04.086.

[49] T. Koida, Amorphous and crystalline In2O3-based transparent conducting films for photovoltaics, Phys. Status Solidi A 214 (2017), 1600464, https://doi.org/10.1002/pssa.201600464.

[50] S. De Wolf, A. Descoeudres, Z.C. Holman, C. Ballif, High-efficiency silicon heterojunction solar cells: a review, Green 2 (2012) 7–24, https://doi.org/10.1515/green-2011-0018.

[51] A. Valla, P. Carroy, F. Ozanne, D. Muñoz, Understanding the role of mobility of ITO films for silicon heterojunction solar cell applications, Sol. Energy Mater. Sol. Cells 157 (2016) 874–880, https://doi.org/10.1016/j.solmat.2016.08.002.

[52] Z.C. Holman, A. Descoeudres, L. Barraud, F.Z. Fernandez, J.P. Seif, S.D. Wolf, C. Ballif, Current losses at the front of silicon heterojunction solar cells, IEEE J. Photovolt. 2 (2012) 7–15, https://doi.org/10.1109/JPHOTOV.2011.2174967.

[53] G. Haacke, New figure of merit for transparent conductors, J. Appl. Phys. 47 (1976) 4086–4089, https://doi.org/10.1063/1.323240.

[54] D. Lachenal, D. Baetzner, W. Frammelsberger, B. Legradic, J. Meixenberger, P. Papet, B. Strahm, G. Wahli, Heterojunction and passivated contacts: a simple method to extract both n/tco and p/tco contacts resistivity, Energy Proc. 92 (2016) 932–938, https://doi.org/10.1016/j.egypro.2016.07.104.

[55] M. Leilaeioun, W. Weigand, M. Boccard, Z.J. Yu, K. Fisher, Z.C. Holman, Contact resistivity of the p-type amorphous silicon hole contact in silicon heterojunction solar cells, IEEE J. Photovolt. 10 (2020) 54–62, https://doi.org/10.1109/JPHOTOV.2019.2949430.

[56] K.U. Ritzau, M. Bivour, S. Schröer, H. Steinkemper, P. Reinecke, F. Wagner, M. Hermle, TCO work function related transport losses at the a-Si:H/TCO-contact in SHJ solar cells, Sol. Energy Mater. Sol. Cells 131 (2014) 9–13, https://doi.org/10.1016/j.solmat.2014.06.026.

[57] M. Bivour, Silicon Heterojunction Solar Cells: Analysis and Basic Understanding, Fraunhofer Verlag, 2017.

[58] L. Zhao, C.L. Zhou, H.L. Li, H.W. Diao, W.J. Wang, Role of the work function of transparent conductive oxide on the performance of amorphous/crystalline silicon heterojunction solar cells studied by computer simulation, Phys. Status Solidi A 205 (2008) 1215–1221, https://doi.org/10.1002/pssa.200723276.

[59] M. Bivour, C. Reichel, M. Hermle, S.W. Glunz, Improving the a-Si:H(p) rear emitter contact of n-type silicon solar cells, Sol. Energy Mater. Sol. Cells 106 (2012) 11–16, https://doi.org/10.1016/j.solmat.2012.06.036.

[60] H. Tasaki, W.Y. Kim, M. Hallerdt, M. Konagai, K. Takahashi, Computer simulation model of the effects of interface states on high-performance amorphous silicon solar cells, J. Appl. Phys. 63 (1988) 550–560, https://doi.org/10.1063/1.340085.

[61] F. Feldmann, K.-U. Ritzau, M. Bivour, A. Moldovan, S. Modi, J. Temmler, M. Hermle, S.W. Glunz, High and low work function materials for passivated contacts, Energy Proc. 77 (2015) 263–270, https://doi.org/10.1016/j.egypro.2015.07.037.

[62] C. Battaglia, X. Yin, M. Zheng, I.D. Sharp, T. Chen, S. McDonnell, A. Azcatl, C. Carraro, B. Ma, R. Maboudian, R.M. Wallace, A. Javey, Hole selective MoOx contact for silicon solar cells, Nano Lett. 14 (2014) 967–971, https://doi.org/10.1021/nl404389u.

[63] C. Battaglia, S.M.d. Nicolás, S.D. Wolf, X. Yin, M. Zheng, C. Ballif, A. Javey, Silicon heterojunction solar cell with passivated hole selective MoOx contact, Appl. Phys. Lett. 104 (2014), 113902, https://doi.org/10.1063/1.4868880.

[64] M. Mews, A. Lemaire, L. Korte, Sputtered tungsten oxide as hole contact for silicon heterojunction solar cells, IEEE J. Photovolt. 7 (2017) 1209–1215, https://doi.org/10.1109/JPHOTOV.2017.2714193.

[65] M. Bivour, J. Temmler, H. Steinkemper, M. Hermle, Molybdenum and tungsten oxide: high work function wide band gap contact materials for hole selective contacts of silicon solar cells, Sol. Energy Mater. Sol. Cells 142 (2015) 34–41, https://doi.org/10.1016/j.solmat.2015.05.031.

[66] L.G. Gerling, S. Mahato, A. Morales-Vilches, G. Masmitja, P. Ortega, C. Voz, R. Alcubilla, J. Puigdollers, Transition metal oxides as hole-selective contacts in silicon heterojunctions solar cells, Sol. Energy Mater. Sol. Cells 145 (2016) 109–115, https://doi.org/10.1016/j.solmat.2015.08.028.

[67] C. Luderer, C. Messmer, M. Hermle, M. Bivour, Transport losses at the TCO/a-Si:H/c-Si heterojunction: influence of different layers and annealing, IEEE J. Photovolt. 10 (2020) 952–958, https://doi.org/10.1109/JPHOTOV.2020.2983989.

[68] G. Nogay, J.P. Seif, Y. Riesen, A. Tomasi, Q. Jeangros, N. Wyrsch, F. Haug, S.D. Wolf, C. Ballif, Nanocrystalline silicon carrier collectors for silicon heterojunction solar cells and impact on low-temperature device characteristics, IEEE J. Photovolt. 6 (2016) 1654–1662, https://doi.org/10.1109/JPHOTOV.2016.2604574.

[69] D. Pysch, C. Meinhard, N.-P. Harder, M. Hermle, S.W. Glunz, Analysis and optimization approach for the doped amorphous layers of silicon heterojunction solar cells, J. Appl. Phys. 110 (2011), 094516, https://doi.org/10.1063/1.3650255.

[70] C. Luderer, L. Tutsch, C. Messmer, M. Hermle, M. Bivour, Influence of TCO and a-Si:H doping on SHJ contact resistivity, IEEE J. Photovolt. 11 (2021) 329–336, https://doi.org/10.1109/JPHOTOV.2021.3051206.

[71] J.P. Seif, A. Descoeudres, G. Nogay, S. Hänni, S.M.d. Nicolas, N. Holm, J. Geissbühler, A. Hessler-Wyser, M. Duchamp, R.E. Dunin-Borkowski, M. Ledinsky, S.D. Wolf, C. Ballif, Strategies for doped nanocrystalline silicon integration in silicon heterojunction solar cells, IEEE J. Photovolt. 6 (2016) 1132–1140, https://doi.org/10.1109/JPHOTOV.2016.2571619.

[72] Y. Zhao, P. Procel, C. Han, L. Mazzarella, G. Yang, A. Weeber, M. Zeman, O. Isabella, Design and optimization of hole collectors based on nc-SiOx:H for high-efficiency silicon heterojunction solar cells, Sol. Energy Mater. Sol. Cells 219 (2021), 110779, https://doi.org/10.1016/j.solmat.2020.110779.

[73] P. Procel, H. Xu, A. Saez, C. Ruiz-Tobon, L. Mazzarella, Y. Zhao, C. Han, G. Yang, M. Zeman, O. Isabella, The role of heterointerfaces and subgap energy states on transport mechanisms in silicon heterojunction solar cells, Prog. Photovolt. Res. Appl. 28 (2020) 935–945, https://doi.org/10.1002/pip.3300.

[74] C. Messmer, M. Bivour, C. Luderer, L. Tutsch, J. Schön, M. Hermle, Influence of interfacial oxides at TCO/doped Si thin film contacts on the charge carrier transport of passivating contacts, IEEE J. Photovolt. 10 (2020) 343–350, https://doi.org/10.1109/JPHOTOV.2019.2957672.

[75] J. Schube, Metallization of Silicon Solar Cells with Passivating Contacts, Universität Freiburg, 2020.

[76] D.K. Schroder, D.L. Meier, Solar cell contact resistance – a review, IEEE Trans. Electron. Dev. 31 (1984) 637–647, https://doi.org/10.1109/T-ED.1984.21583.

[77] J. Schube, L. Tutsch, T. Fellmeth, M. Bivour, F. Feldmann, T. Hatt, F. Maier, R. Keding, F. Clement, S.W. Glunz, Low-resistivity screen-printed contacts on indium tin oxide layers for silicon solar cells with passivating contacts, IEEE J. Photovolt. 8 (2018) 1208–1214, https://doi.org/10.1109/JPHOTOV.2018.2859768.

[78] E. Kobayashi, Y. Watabe, T. Yamamoto, Y. Yamada, Cerium oxide and hydrogen co-doped indium oxide films for high-efficiency silicon heterojunction solar cells, Sol. Energy Mater. Sol. Cells 149 (2016) 75–80, https://doi.org/10.1016/j.solmat.2016.01.005.

[79] B. Demaurex, J.P. Seif, S. Smit, B. Macco, W.M.M. Kessels, J. Geissbühler, S.D. Wolf, C. Ballif, Atomic-layer-deposited transparent electrodes for silicon heterojunction solar cells, IEEE J. Photovolt. 4 (2014) 1387–1396, https://doi.org/10.1109/JPHOTOV.2014.2344771.

[80] B. Macco, B.W. H.v. d. Loo, J. Melskens, S. Smit, W.M.M.E. Kessels, Status and prospects for atomic layer deposited metal oxide thin films in passivating contacts for c-Si photovoltaics, in: 2016 IEEE 43rd Photovoltaic Specialists Conference (PVSC), 5-10 June 2016, 2016, pp. 2473–2478.

[81] Y. Wu, B. Macco, D. Vanhemel, S. Kölling, M.A. Verheijen, P.M. Koenraad, W.M.M. Kessels, F. Roozeboom, Atomic layer deposition of In_2O_3:H from InCp and H_2O/O_2: microstructure and isotope labeling studies, ACS Appl. Mater. Interfaces 9 (2017) 592–601, https://doi.org/10.1021/acsami.6b13560.

[82] H.-K. Kim, D.-G. Kim, K.-S. Lee, M.-S. Huh, S.H. Jeong, K.I. Kim, T.-Y. Seong, Plasma damage-free sputtering of indium tin oxide cathode layers for top-emitting organic light-emitting diodes, Appl. Phys. Lett. 86 (2005), 183503, https://doi.org/10.1063/1.1923182.

[83] V. Linss, M. Bivour, H. Iwata, K. Ortner, Comparison of low damage sputter deposition techniques to enable the application of very thin a-Si passivation films, AIP Conf. Proc. 2147 (2019), 040009, https://doi.org/10.1063/1.5123836.

[84] A.H.T. Le, V.A. Dao, D.P. Pham, S. Kim, S. Dutta, C.P. Thi Nguyen, Y. Lee, Y. Kim, J. Yi, Damage to passivation contact in silicon heterojunction solar cells by ITO sputtering under various plasma excitation modes, Sol. Energy Mater. Sol. Cells 192 (2019) 36–43, https://doi.org/10.1016/j.solmat.2018.12.001.

[85] S. De Wolf, B. Demaurex, A. Descoeudres, C. Ballif, Very fast light-induced degradation of a-Si:H/c-Si(100) interfaces, Phys. Rev. B 83 (2011), 233301, https://doi.org/10.1103/PhysRevB.83.233301.

[86] B. Demaurex, S.D. Wolf, A. Descoeudres, Z.C. Holman, C. Ballif, Damage at hydrogenated amorphous/crystalline silicon interfaces by indium tin oxide overlayer sputtering, Appl. Phys. Lett. 101 (2012), 171604, https://doi.org/10.1063/1.4764529.

[87] A. Illiberi, P. Kudlacek, A.H.M. Smets, M. Creatore, M.C. M.v. d. Sanden, Effect of ion bombardment on the a-Si:H based surface passivation of c-Si surfaces, Appl. Phys. Lett. 98 (2011), 242115, https://doi.org/10.1063/1.3601485.

[88] P.M. Gevers, J.J.H. Gielis, H.C.W. Beijerinck, M.C. M.v. d. Sanden, W.M.M. Kessels, Amorphization of Si(100) by Ar+-ion bombardment studied with spectroscopic and time-resolved second-harmonic generation, J. Vac. Sci. Technol. A 28 (2010) 293–301, https://doi.org/10.1116/1.3305812.

[89] A. Plagemann, K. Ellmer, K. Wiesemann, Laterally resolved ion-distribution functions at the substrate position during magnetron sputtering of indium-tin oxide films, J. Vac. Sci. Technol. A 25 (2007) 1341–1350, https://doi.org/10.1116/1.2753843.

[90] M. Stutzmann, W.B. Jackson, C.C. Tsai, Light-induced metastable defects in hydrogenated amorphous silicon: a systematic study, Phys. Rev. B 32 (1985) 23–47, https://doi.org/10.1103/PhysRevB.32.23.

[91] I. Hirabayashi, K. Morigaki, S. Nitta, New evidence for defect creation by high optical excitation in glow discharge amorphous silicon, Jpn. J. Appl. Phys. 19 (1980) L357–L360, https://doi.org/10.1143/jjap.19.l357.

[92] C.G. V.d. Walle, R. Street, Silicon-hydrogen bonding and hydrogen diffusion in amorphous silicon, Phys. Rev. B Condens. Matter 51 (1995) 10615–10618, https://doi.org/10.1557/PROC-377-389.

[93] R.B. Wehrspohn, S.C. Deane, I.D. French, I. Gale, J. Hewett, M.J. Powell, J. Robertson, Relative importance of the Si–Si bond and Si–H bond for the stability of amorphous silicon thin film transistors, J. Appl. Phys. 87 (2000) 144–154, https://doi.org/10.1063/1.371836.

[94] B.M. Meiners, D. Borchert, S. Hohage, S. Holinksi, P. Schäfer, Degradation of hydrogenated amorphous silicon passivation films caused by sputtering deposition, Phys. Status Solidi A 212 (2015) 1817–1822, https://doi.org/10.1002/pssa.201431923.
[95] L. Tutsch, Implementing Sputter-Deposited Transparent Conductive Metal Oxides into Passivating Contacts for Silicon Solar Cells, Dissertation, Universität Freiburg, 2020.
[96] T. Welzel, K. Ellmer, Negative ions in reactive magnetron sputtering, Vak. Forsch. Prax. 25 (2013) 52–56, https://doi.org/10.1002/vipr.201300518.
[97] M. Bender, J. Trube, J. Stollenwerk, Characterization of a RF/dc-magnetron discharge for the sputter deposition of transparent and highly conductive ITO films, Appl. Phys. A 69 (1999) 397–401, https://doi.org/10.1007/s003390051021.
[98] M. Huang, Z. Hameiri, A.G. Aberle, T. Mueller, Comparative study of amorphous indium tin oxide prepared by pulsed-DC and unbalanced RF magnetron sputtering at low power and low temperature conditions for heterojunction silicon wafer solar cell applications, Vacuum 119 (2015) 68–76, https://doi.org/10.1016/j.vacuum.2015.04.032.
[99] U.K. Das, M.Z. Burrows, M. Lu, S. Bowden, R.W. Birkmire, Surface passivation and heterojunction cells on Si (100) and (111) wafers using DC and RF plasma deposited Si:H thin films, Appl. Phys. Lett. 92 (2008), 063504, https://doi.org/10.1063/1.2857465.
[100] H. Fujiwara, M. Kondo, Impact of epitaxial growth at the heterointerface of a-Si:H/c-Si solar cells, Appl. Phys. Lett. 90 (2007), 013503, https://doi.org/10.1063/1.2426900.
[101] S.D. Wolf, S. Olibet, C. Ballif, Stretched-exponential a-Si:H/c-Si interface recombination decay, Appl. Phys. Lett. 93 (2008), 032101, https://doi.org/10.1063/1.2956668.
[102] Y. Kuang, B. Macco, B. Karasulu, C.K. Ande, P.C.P. Bronsveld, M.A. Verheijen, Y. Wu, W.M.M. Kessels, R.E.I. Schropp, Towards the implementation of atomic layer deposited In_2O_3:H in silicon heterojunction solar cells, Sol. Energy Mater. Sol. Cells 163 (2017) 43–50, https://doi.org/10.1016/j.solmat.2017.01.011.
[103] J. Jeurink, F. Wagner, S. Park, L. Kroely, W. Wolke, MF-Sputtered AZO for a-Si SHJ solar cells, Energy Proc. 55 (2014) 777–785, https://doi.org/10.1016/j.egypro.2014.08.059.
[104] A. Kanevce, W.K. Metzger, The role of amorphous silicon and tunneling in heterojunction with intrinsic thin layer (HIT) solar cells, J. Appl. Phys. 105 (2009), 094507, https://doi.org/10.1063/1.3106642.
[105] S.Q. Hussain, W.-K. Oh, S. Ahn, A.H.T. Le, S. Kim, Y. Lee, J. Yi, RF magnetron sputtered indium tin oxide films with high transmittance and work function for a-Si:H/c-Si heterojunction solar cells, Vacuum 101 (2014) 18–21, https://doi.org/10.1016/j.vacuum.2013.07.004.
[106] S. Kirner, M. Hartig, L. Mazzarella, L. Korte, T. Frijnts, H. Scherg-Kurmes, S. Ring, B. Stannowski, B. Rech, R. Schlatmann, The influence of ITO dopant density on J-V characteristics of silicon heterojunction solar cells: experiments and simulations, Energy Proc. 77 (2015) 725–732, https://doi.org/10.1016/j.egypro.2015.07.103.
[107] M.L. Addonizio, E. Gambale, A. Antonaia, Microstructure evolution of room-temperature-sputtered ITO films suitable for silicon heterojunction solar cells, Curr. Appl. Phys. 20 (2020) 953–960, https://doi.org/10.1016/j.cap.2020.06.007.
[108] H. Li, S. Yin, G. Dong, G. Cui, M. Chen, J. Chen, X. Xu, L. Feng, J. Zhang, C. Yu, In-Sn oxide bilayer transparent conductive film by DC magnetron sputtering for silicon heterojunction solar cells, IEEE J. Photovolt. 11 (2021) 312–318, https://doi.org/10.1109/JPHOTOV.2020.3048259.
[109] H.P. Zhou, S. Xu, Z. Zhao, Y. Xiang, Inductively coupled hydrogen plasma processing of AZO thin films for heterojunction solar cell applications, J. Alloys Compd. 610 (2014) 107–112, https://doi.org/10.1016/j.jallcom.2014.04.216.
[110] J. Kim, J.-H. Yun, Y.C. Park, W.A. Anderson, Transparent and crystalline Al-doped ZnO film-embedded heterojunction Si solar cell, Mater. Lett. 75 (2012) 99–101, https://doi.org/10.1016/j.matlet.2012.01.144.
[111] R. Pietruszka, B.S. Witkowski, E. Zielony, K. Gwozdz, E. Placzek-Popko, M. Godlewski, ZnO/Si heterojunction solar cell fabricated by atomic layer deposition and hydrothermal methods, Sol. Energy 155 (2017) 1282–1288, https://doi.org/10.1016/j.solener.2017.07.071.
[112] L.L. Senaud, G. Christmann, A. Descoeudres, J. Geissbühler, L. Barraud, N. Badel, C. Allebé, S. Nicolay, M. Despeisse, B. Paviet-Salomon, C. Ballif, Aluminium-doped zinc oxide rear reflectors for high-efficiency silicon heterojunction solar cells, IEEE J. Photovolt. 9 (2019) 1217–1224, https://doi.org/10.1109/JPHOTOV.2019.2926860.
[113] T.L. Chen, D.S. Ghosh, D. Krautz, S. Cheylan, V. Pruneri, Highly stable Al-doped ZnO transparent conductors using an oxidized ultrathin metal capping layer at its percolation thickness, Appl. Phys. Lett. 99 (2011), 093302, https://doi.org/10.1063/1.3631674.
[114] J. Wang, C. Meng, H. Liu, Y. Hu, L. Zhao, W. Wang, X. Xu, Y. Zhang, H. Yan, Application of indium tin oxide/aluminum-doped zinc oxide transparent conductive oxide stack films in silicon heterojunction solar cells, ACS Appl. Energy Mater. 4 (2021) 13586–13592, https://doi.org/10.1021/acsaem.1c02209.
[115] Y. Wang, X. Zhang, L. Bai, Q. Huang, C. Wei, Y. Zhao, Effective light trapping in thin film silicon solar cells from textured Al doped ZnO substrates with broad surface feature distributions, Appl. Phys. Lett. 100 (2012), 263508, https://doi.org/10.1063/1.4731775.
[116] T.G. Allen, J. Bullock, X. Yang, A. Javey, S. De Wolf, Passivating contacts for crystalline silicon solar cells, Nat. Energy 4 (2019) 914–928, https://doi.org/10.1038/s41560-019-0463-6.
[117] W. Duan, K. Bittkau, A. Lambertz, K. Qiu, Z. Yao, P. Steuter, D. Qiu, U. Rau, K. Ding, Improved infrared light management with transparent conductive oxide/amorphous silicon back reflector in high-efficiency silicon heterojunction solar cells, Sol. RRL 5 (2021), 2000576, https://doi.org/10.1002/solr.202000576.
[118] S. Li, M. Pomaska, A. Lambertz, W. Duan, K. Bittkau, D. Qiu, Z. Yao, M. Luysberg, P. Steuter, M. Köhler, K. Qiu, R. Hong, H. Shen, F. Finger, T. Kirchartz, U. Rau, K. Ding, Transparent-conductive-oxide-free front contacts for high-efficiency silicon heterojunction solar cells, Joule 5 (2021) 1535–1547, https://doi.org/10.1016/j.joule.2021.04.004.
[119] A. Cruz, E.-C. Wang, A.B. Morales-Vilches, D. Meza, S. Neubert, B. Szyszka, R. Schlatmann, B. Stannowski, Effect of front TCO on the performance of rear-junction silicon heterojunction solar cells: insights from simulations and experiments, Sol. Energy Mater. Sol. Cells 195 (2019) 339–345, https://doi.org/10.1016/j.solmat.2019.01.047.
[120] L. Barraud, Z.C. Holman, N. Badel, P. Reiss, A. Descoeudres, C. Battaglia, S. De Wolf, C. Ballif, Hydrogen-doped indium oxide/indium tin oxide bilayers for high-efficiency silicon heterojunction solar cells, Sol. Energy Mater. Sol. Cells 115 (2013) 151–156, https://doi.org/10.1016/j.solmat.2013.03.024.
[121] T. Koida, H. Fujiwara, M. Kondo, Reduction of optical loss in hydrogenated amorphous silicon/crystalline silicon heterojunction solar cells by high-mobility hydrogen-doped In_2O_3 transparent conductive oxide, Appl. Phys. Express 1 (2008), 041501, https://doi.org/10.1143/APEX.1.041501.
[122] T. Koida, H. Fujiwara, M. Kondo, High-mobility hydrogen-doped In2O3 transparent conductive oxide for a-Si:H/c-Si heterojunction solar cells, Sol. Energy Mater. Sol. Cells 93 (2009) 851–854, https://doi.org/10.1016/j.solmat.2008.09.047.
[123] V.A. Dao, S. Kim, Y. Lee, S. Kim, J. Park, S. Ahn, J. Yi, High-efficiency heterojunction with intrinsic thin-layer solar cells: a review, Curr. Photovolt. Res. 1 (2013) 73–81, https://doi.org/10.21218/CPR.2013.1.2.073.
[124] T. Nishihara, K. Muramatsu, K. Nakamura, Y. Ohshita, S. Yasuno, H. Kanai, Y. Hara, Y. Hibino, H. Kojima, A. Ogura, Investigation of the chemical reaction between silver electrodes and transparent conductive oxide films for the improvement of fill factor of silicon heterojunction solar cells, ECS J. Solid State Sci. Technol. 10 (2021), 055013, https://doi.org/10.1149/2162-8777/abffae.
[125] S. Li, Z. Shi, Z. Tang, X. Li, Comparison of ITO, In2O3:Zn and In2O3:H transparent conductive oxides as front electrodes for silicon heterojunction solar cell applications, Vacuum 145 (2017) 262–267, https://doi.org/10.1016/j.vacuum.2017.09.011.
[126] J. Geissbühler, J. Werner, S.M.d. Nicolas, L. Barraud, A. Hessler-Wyser, M. Despeisse, S. Nicolay, A. Tomasi, B. Niesen, S.D. Wolf, C. Ballif, 22.5% efficient silicon heterojunction solar cell with molybdenum oxide hole collector, Appl. Phys. Lett. 107 (2015), 081601, https://doi.org/10.1063/1.4928747.
[127] Y. Liu, S. Zhu, R. Wei, L. Hu, X. Tang, J. Yang, W. Song, J. Dai, X. Zhu, Y. Sun, Solution processed W-doped In_2O_3 thin films with high carrier mobility, Ceram. Int. 46 (2020) 2173–2177, https://doi.org/10.1016/j.ceramint.2019.09.201.
[128] C. Han, Y. Zhao, L. Mazzarella, R. Santbergen, A. Montes, P. Procel, G. Yang, X. Zhang, M. Zeman, O. Isabella, Room-temperature sputtered tungsten-doped indium oxide for improved current in silicon heterojunction solar cells, Sol. Energy Mater. Sol. Cells 227 (2021), 111082, https://doi.org/10.1016/j.solmat.2021.111082.
[129] S. Huang, W. Liu, X. Li, Z. Li, Z. Wu, W. Huang, Y. Yang, K. Jiang, J. Shi, L. Zhang, F. Meng, Z. Liu, Prolonged annealing improves hole transport of silicon heterojunction solar cells, Phys. Status Solidi RRL 15 (2021), 2100015, https://doi.org/10.1002/pssr.202100015.
[130] E. Kobayashi, N. Nakamura, Y. Watabe, Reduction of optical and electrical losses in silicon heterojunction solar cells by hydrogenated tungsten-doped In2O3, in: Proc 27th European Photovoltaic Solar Energy Conference, 2012, pp. 1619–1623.
[131] J. Li, J. Yu, T. Chen, H. Zhang, Q. Wang, P. Wang, Y. Huang, In-situ formation of indium seed layer for copper metallization of silicon heterojunction solar cells, Sol. Energy Mater. Sol. Cells 204 (2020), 110243, https://doi.org/10.1016/j.solmat.2019.110243.
[132] F. Meng, J. Shi, Z. Liu, Y. Cui, Z. Lu, Z. Feng, High mobility transparent conductive W-doped In_2O_3 thin films prepared at low substrate temperature and its application to solar cells, Sol. Energy Mater. Sol. Cells 122 (2014) 70–74, https://doi.org/10.1016/j.solmat.2013.11.030.
[133] W. Huang, J. Shi, Y. Liu, Z. Wu, F. Meng, Z. Liu, High-performance Ti and W co-doped indium oxide films for silicon heterojunction solar cells prepared by reactive plasma deposition, J. Power Sources 506 (2021), 230101, https://doi.org/10.1016/j.jpowsour.2021.230101.
[134] F. Meng, J. Shi, L. Shen, L. Zhang, J. Liu, Y. Liu, J. Yu, J. Bao, Z. Liu, Characterization of transparent conductive oxide films and their effect on amorphous/crystalline silicon heterojunction solar cells, Jpn. J. Appl. Phys. 56 (2017), 04CS09, https://doi.org/10.7567/JJAP.56.04CS09.
[135] J. Yu, J. Bian, W. Duan, Y. Liu, J. Shi, F. Meng, Z. Liu, Tungsten doped indium oxide film: ready for bifacial copper metallization of silicon heterojunction solar cell, Sol. Energy Mater. Sol. Cells 144 (2016) 359–363, https://doi.org/10.1016/j.solmat.2015.09.033.

[136] J. Yu, J. Bian, Y. Liu, F. Meng, Z. Liu, Patterning and formation of copper electroplated contact for bifacial silicon hetero-junction solar cell, Sol. Energy 146 (2017) 44–49, https://doi.org/10.1016/j.solener.2017.02.022.
[137] W. Liu, J. Shi, L. Zhang, A. Han, S. Huang, X. Li, J. Peng, Y. Yang, Y. Gao, J. Yu, K. Jiang, X. Yang, Z. Li, W. Zhao, J. Du, X. Song, J. Yin, J. Wang, Y. Yu, Q. Shi, Z. Ma, H. Zhang, J. Ling, L. Xu, J. Kang, F. Xu, J. Liu, H. Liu, Y. Xie, F. Meng, S. De Wolf, F. Laquai, Z. Di, Z. Liu, Light-induced activation of boron doping in hydrogenated amorphous silicon for over 25% efficiency silicon solar cells, Nat. Energy 7 (2022) 427–437, https://doi.org/10.1038/s41560-022-01018-5.
[138] P.-C. Hsiao, W. Zhang, Z. Li, U. Römer, A. Lennon, Direct copper plating to IWO for silicon heterojunction solar cells, in: 2018 IEEE 7th World Conference on Photovoltaic Energy Conversion (WCPEC) (A Joint Conference of 45th IEEE PVSC, 28th PVSEC & 34th EU PVSEC), 10–15 June 2018, 2018, pp. 3719–3721.
[139] L. Tutsch, H. Sai, T. Matsui, M. Bivour, M. Hermle, T. Koida, The sputter deposition of broadband transparent and highly conductive cerium and hydrogen co-doped indium oxide and its transfer to silicon heterojunction solar cells, Prog. Photovolt. Res. Appl. 29 (2021) 835–845, https://doi.org/10.1002/pip.3388.
[140] H. Li, S. Yin, G. Dong, G. Cui, C. Lei, Y. Li, X. Xu, L. Feng, J. Zhang, C. Yu, Effect of humidity on optical and electrical properties of Zr-doped In2O3 and a new structure for transparent electrode of silicon heterojunction solar cell, Sol. Energy Mater. Sol. Cells 196 (2020) 125–131, https://doi.org/10.1016/j.solener.2019.12.017.
[141] M. Morales-Masis, E. Rucavado, R. Monnard, L. Barraud, J. Holovský, M. Despeisse, M. Boccard, C. Ballif, Highly conductive and broadband transparent Zr-doped In2O3 as front electrode for solar cells, IEEE J. Photovolt. 8 (2018) 1202–1207, https://doi.org/10.1109/JPHOTOV.2018.2851306.
[142] M. Ahrlich, O. Sergeev, M. Juilfs, A. Neumüller, M. Vehse, C. Agert, Improved light management in silicon heterojunction solar cells by application of a ZnO nanorod antireflective layer, Energy Proc. 92 (2016) 284–290, https://doi.org/10.1016/j.egypro.2016.07.080.
[143] Z. Wu, W. Duan, A. Lambertz, D. Qiu, M. Pomaska, Z. Yao, U. Rau, L. Zhang, Z. Liu, K. Ding, Low-resistivity p-type a-Si:H/AZO hole contact in high-efficiency silicon heterojunction solar cells, Appl. Surf. Sci. 542 (2021), 148749, https://doi.org/10.1016/j.apsusc.2020.148749.
[144] J.-P. Niemelä, B. Macco, L. Barraud, A. Descoeudres, N. Badel, M. Despeisse, G. Christmann, S. Nicolay, C. Ballif, W.M.M. Kessels, M. Creatore, Rear-emitter silicon heterojunction solar cells with atomic layer deposited ZnO:Al serving as an alternative transparent conducting oxide to In_2O_3:Sn, Sol. Energy Mater. Sol. Cells 200 (2019), 109953, https://doi.org/10.1016/j.solmat.2019.109953.
[145] A.B. Morales-Vilches, A. Cruz, S. Pingel, S. Neubert, L. Mazzarella, D. Meza, L. Korte, R. Schlatmann, B. Stannowski, ITO-free silicon heterojunction solar cells with ZnO:Al/SiO_2 front electrodes reaching a conversion efficiency of 23, IEEE J. Photovolt. 9 (2019) 34–39, https://doi.org/10.1109/JPHOTOV.2018.2873307.
[146] H. Kawazoe, M. Yasukawa, H. Hyodo, M. Kurita, H. Yanagi, H. Hosono, P-type electrical conduction in transparent thin films of $CuAlO_2$, Nature 389 (1997) 939–942, https://doi.org/10.1038/40087.
[147] L. Lancellotti, E. Bobeico, M. Della Noce, L.V. Mercaldo, I. Usatii, P. Delli Veneri, G.V. Bianco, A. Sacchetti, G. Bruno, Graphene as non conventional transparent conductive electrode in silicon heterojunction solar cells, Appl. Surf. Sci. 525 (2020), 146443, https://doi.org/10.1016/j.apsusc.2020.146443.
[148] S. Maity, K. Sarkar, P. Kumar, A progressive journey into 2D-chalcogenide/carbide/nitride-based broadband photodetectors: recent developments and future perspectives, J. Mater. Chem. C 9 (2021) 14532–14572, https://doi.org/10.1039/D1TC02820K.
[149] R. Nagarajan, A.D. Draeseke, A.W. Sleight, J. Tate, p-type conductivity in $CuCr_{1-x}$ $MgxO_2$ films and powders, J. Appl. Phys. 89 (2001) 8022–8025, https://doi.org/10.1063/1.1372636.
[150] A. Zakery, S.R. Elliott, Optical properties and applications of chalcogenide glasses: a review, J. Non Cryst. Solids 330 (2003) 1–12, https://doi.org/10.1016/j.jnoncrysol.2003.08.064.
[151] M. Zeng, Y. Li, Recent advances in heterogeneous electrocatalysts for the hydrogen evolution reaction, J. Mater. Chem. 3 (2015) 14942–14962, https://doi.org/10.1039/C5TA02974K.
[152] M.Q. Khokhar, S.Q. Hussain, S. Kim, S. Lee, D.P. Pham, Y. Kim, E.-C. Cho, J. Yi, Review of rear emitter silicon heterojunction solar cells, Trans. Electr. Electron. Mater. 21 (2020) 138–143, https://doi.org/10.1007/s42341-020-00172-5.
[153] M. Bivour, H. Steinkemper, J. Jeurink, S. Schröer, M. Hermle, Rear emitter silicon heterojunction solar cells: fewer restrictions on the optoelectrical properties of front side TCOs, Energy Proc. 55 (2014) 229–234, https://doi.org/10.1016/j.egypro.2014.08.035.
[154] A. Cruz, D. Erfurt, R. Köhler, M. Dimer, E. Schneiderlöchner, B. Stannowski, Industrial TCOs for SHJ solar cells: approaches for optimizing performance and cost, Photovolt. Int. 44 (2020) 86–96.
[155] J. Shin, H. Kim, K.H. Song, J. Choe, Synthesis of silver-coated copper particles with thermal oxidation stability for a solar cell conductive paste, Chem. Lett. 44 (2015) 1223–1225, https://doi.org/10.1246/cl.150424.
[156] K. Chung, J. Bang, A. Thacharon, H.Y. Song, S.H. Kang, W.-S. Jang, N. Dhull, D. Thapa, C.M. Ajmal, B. Song, S.-G. Lee, Z. Wang, A. Jetybayeva, S. Hong, K.H. Lee, E.J. Cho, S. Baik, S.H. Oh, Y.-M. Kim, Y.H. Lee, S.-G. Kim, S.W. Kim, Non-oxidized bare copper nanoparticles with surface excess electrons in air, Nat. Nanotech. 17 (2022) 285–291, https://doi.org/10.1038/s41565-021-01070-4.
[157] D. Meza, A. Cruz, A.B. Morales-Vilches, L. Korte, B. Stannowski, Aluminum-doped zinc oxide as front electrode for rear emitter silicon heterojunction solar cells with high efficiency, Appl. Sci. 9 (2019) 862, https://doi.org/10.3390/app9050862.
[158] P.H. Chen, W.J. Chen, J.Y. Tseng, Thermal stability of the copper and the AZO layer on textured silicon, Coatings 11 (2021) 1546, https://doi.org/10.3390/coatings11121546.

Further reading

[159] G. Agostinelli, A. Delabie, P. Vitanov, Z. Alexieva, H.F.W. Dekkers, S. De Wolf, G. Beaucarne, Very low surface recombination velocities on p-type silicon wafers passivated with a dielectric with fixed negative charge, Sol. Energy Mater. Sol. Cells 90 (2006) 3438–3443, https://doi.org/10.1016/j.solmat.2006.04.014.